THE UNIVERSITY OF MICHIGAN

COLLEGE OF ENGINEERING

Departments of

Aerospace Engineering

Meteorology and Oceanography

Technical Report

AN EXPERIMENTAL FOURIER-TRANSFORM ASYMMETRICAL

INTERFEROMETER FOR ATMOSPHERIC RADIATION MEASUREMENTS

L. W. Chaney

ORA Project 05863

under contract with:

NATIONAL AERONAUTICS AND SPACE ADMINISTRATION

CONTRACT NO. NASr-54(03)

WASHINGTON, D. C.

administered through

OFFICE OF RESEARCH ADMINISTRATION   ANN ARBOR

December 1969

ACKNOWLEDGEMENTS

The work described in this report was completed as a result of the dedicated help of the other members of the laboratory staff. Special thanks go to Fred Bartman who has directed the atmospheric radiation studies and given many helpful comments on the report itself.

The author is particularly grateful to Douglas Robinson who carefully performed many of the optical and electrical tests on the instrument. Gunar Liepins was responsible for the balloon flight operation and designed the in-flight calibration equipment. Wan Lee wrote the computer programs and carried out the numerous computations. The inversion solution is due to the courtesy of S. Roland Drayson.

TABLE OF CONTENTS

LIST OF TABLES

LIST OF ILLUSTRATIONS

ABSTRACT

An experimental Fourier transform spectrometer was modified to operate in an asymmetrical mode for the purpose of increasing the resolution. The computational problems associated with the asymmetrical mode are described.

The instrument was flown on a high altitude balloon flight on November 20, 1968 and some of the data obtained during the flight is presented.

1.0 Introduction

The High Altitude Engineering Laboratory (HAEL) began experimenting with the application of Fourier Spectroscopy to atmospheric radiation measurements in 1961. The original instrument was a modified Block I-4 flown on a high altitude balloon in June 1963.[1] The results of the flight were very encouraging and lead to the development of a more sophisticated instrument.

The Block I-4, as modified, had a resolution of 50 cm^{-1} and covered the spectral region from 667 to 2000 cm^{-1}. The more sophisticated instrument, later known as the IRIS-A, (Infrared Interferometer Spectrometer) covered the spectral range from 500 to 2000 cm^{-1} with a resolution of 5 cm^{-1} The instrument was developed jointly by HAEL and Goddard Space Flight Center (GSFC) and flown on a high altitude balloon on May 8, 1966.[2]

A contract was awarded to the Texas Instrument Company by GSFC to design a similar interferometer for satellite use. The performance of the satellite instrument was to match that obtained by the experimental unit. The satellite instrument, known as the IRIS-B, was flown on the Nimbus B satellite in April 1968. Unfortunately the satellite failed and was lost at sea. A new Nimbus was constructed and the flight back-up instrument was flown in April 1969. Several spectra have now been received from various parts of the earth and temperature inversions made.[3]

As a part of the satellite interferometer development program, HAEL continued the development of more sophisticated techniques. The techniques investigated were as follows:

(1) A servo control system to maintain the fixed mirror aligned with the moving mirror.

(2) The use of "cat's eye" reflectors in place of the flat mirrors.

(3) The use of a thin film beam splitter in place of the potassium bromide substrate.

(4) The development of asymmetrical interferogram data reduction
techniques.

In October of 1967 plans were made to fly the pre-prototype
model of the satellite instrument on a high altitude balloon. A decision was
also made to fly the experimental interferometer incorporating any of the
feasible modifications. The first three techniques were investigated and
abandoned. The fourth, the development of asymmetrical interferogram
techniques, seemed quite promising. The development continued and the
experimental instrument incorporating the asymmetrical feature was flown
November 20, 1968.

2.0 The basic asymmetric technique.

The technique has been described by Vanasse[4] and is a method
where by the resolution of a given physical interferometer can be essentially
doubled.

A typical interferogram is shown in Fig. 1. The maximum
amplitude of the interferogram occurs at the center of the scan. The inter
ferogram appears to be very close to being symmetrical, but not quite. The
reason for the asymmetry is that there are optical phase shifts at the surface
of the beam splitter and electrical phase shifts associated with the amplifiers
and detector networks. The interferogram can be represented by the
following equation,

$$I(x) = \int_{0}^{\sigma_m} \beta(\sigma) \left[\cos 2\pi \sigma x + \varphi(\sigma) \right] d\sigma$$

The fundamental idea is that the phase shifts, $\varphi(\sigma)$ are a part of the instru-
mentation and fixed. Therefore, if the phase shift as a function of wavenumber
were once measured and corrected the required symmetry could be assumed.

2

If the interferogram were asymmetrical (Fig. 2) it would be necessary to use only one side to calculate the spectrum. Hence, the central maximum could be moved to one side and the distance from the maximum to the end of the scan would be doubled. The spectral resolution is proportional to the reciprocal of the scan length.

The original technique proposed to carry out the phase correction was as follows:[4,5]

(1) Record an asymmetrical interferogram of a warm blackbody.

$$I(x) = \int_O^m \beta \, (\sigma) \left[\cos 2\pi \, \sigma x + \varphi(\sigma) \right] \, d\sigma$$

(2) Apodize the two-sided portion of the interferogram $\pm$ 400 points.

(3) Calculate the low resolution Fourier transform from these points.

(4) Use the sine and cosine components to calculate the phase angle as a function of wavenumber. $\varphi \, (\sigma) = \arctan S/C$.

(5) Use the phase information to generate a convolution function.

$$C(x) = \tilde{e}^{-i \, (\varphi(\sigma) \,)}$$

(6) Convolve the convolution function with the original interferogram to obtain a symmetrical interferogram. (Fig. 2).

$$C(x) * I(x) = I'(x) = \int_O^{\sigma \, m} \beta(\sigma) \, \cos 2\pi \, \sigma x \, d\sigma$$

(7) Calculate the Fourier transform of the symmetrical interferogram. (Fig. 3).

The procedure outlined above was quite satisfactory for obtaining the spectra of blackbodies and can be used for any spectrum that has radiance of the same sign with respect to the reference at all parts of the spectrum being measured. The problems that were encountered in the data reduction arose for two reasons. One, the flight radiance measurements (Fig. 9 and 11) were both positive and negative with respect to the bolometer reference. Two, there was a random shift in the sampling of the infrared interferogram.

3

3.0 Experimental Problems

The instrument was designed to observe both positive and negative radiation with respect to the 0° C reference temperature. Hence, the bi-directional character of the radiation was not a problem. However, the combination of the bi-directional radiation measurement and the sampling "jitter" proved difficult to untangle.

The sampling of the interferogram is determined by the monochromatic interferogram produced by the filtered neon line used as a wavelength reference. The infrared interferogram and the corresponding neon line interferogram are shown in Fig. 4. The construction of the experimental interferometer was such that the infrared signal utilized the entire Michelson mirror, whereas the reference line utilized one edge of the mirror. Consequently, any slight tilting of the mirror due to vibration would cause momentary shifting, "Jitter", of the reference line with respect to the infrared interferogram.

The data reduction plan required the calculation of a single convolution function $C(x)$ derived from a calibration black body. The function $C(x)$ was to be convolved with all interferograms. However, due to the "Jitter" a typical black body interferogram was not as depicted in Fig. 1, but as shown in Fig. 5. The more generalized expression for a black body interferogram is

$$I_{BB}(x) = \int_0^{\sigma_m} \beta(\sigma) \, \text{Cos} \left[2\pi \, \sigma x + \varphi'_{BB}(\sigma) + \varphi''_{BB}(\sigma) \right] \, d\sigma$$

The term, $\varphi'(\sigma)_{BB}$, represents the constant non-linear phase shifts associated with the beam splitter and the electrical filters. The term $\varphi''_{BB}(\sigma)$, represents the linear phase shifts resulting from the displacement in sampling.

$$\varphi''_{BB}(\sigma) = -2\pi \sigma \xi$$

if $\xi =$ the distance from the closest sampling point to the central maximum.

The convolution function

$$C_{BB}(x) = e^{-i[\varphi'_{BB}(\sigma) + \varphi''_{BB})\sigma)]}$$

when convolved with the original interferogram

$$I_{BB}(x) * C_{BB}(x) = I'_{BB}(x) = \int_0^{\sigma m} \beta(\sigma) \cos 2\pi \sigma x \, d\sigma$$

would correct the phase function $[\varphi'_{BB}(\sigma) + \varphi''_{BB}(\sigma)]$.

However, the phase function for a scene interferogram would be

$$\varphi'_s(\sigma) + \varphi''_s(\sigma) \qquad\qquad \text{where}$$

$$\varphi'_s(\sigma) = \varphi'_{BB}(\sigma) \qquad\qquad \text{but}$$

$$\varphi''_s(\sigma) \neq \varphi''_{BB}(\sigma) \text{ o}$$

3.1 Sampling Problem

The sampling problem reduces to the generation of unwanted $\varphi''(\sigma)$ terms.[5]

Theoretically the $\varphi''(\sigma)$ term can be eliminated for each interferogram by interpolating the sampling points and then proceeding as originally planned. The most straight forward interpolation procedure is to measure either ξ or $\varphi''(\sigma)$ and form a convolution function

$$C'(x) = e^{-i \, \tilde{\varphi}'(\sigma)} \qquad\qquad \text{to be}$$

convolved with the original interferogram.

The determination of ξ from the interferogram plots required very careful plotting on a large scale. Hence, we elected to determine $\varphi''(\sigma)$ by examining phase plots calculated from a low resolution spectrum.

The effect on the phase plot of eliminating $\varphi''(\sigma)$ can be observed by comparing Fig. 1 and Fig. 5. The value of $\varphi''(\sigma)$ is zero in Fig. 1 and can be determined by the average slope of the curve in Fig. 5.

The determination of $\varphi''(\sigma)$ for this case is uncomplicated, but in the case of scene interferograms there are other problems.

A typical scene interferogram is shown in Fig. 6. Because of the presence of both positive and negative radiation the central "maximum" is actually smaller than several of the side lobes. Whenever this situation occurred it was necessary to make several low resolution transformations and the corresponding phase plots before correctly identifying the central maximum. Also because of the 180° phase shifts associated with the change in direction of the radiation, the isolation of $\varphi''(\sigma)$(Fig. 6) was often difficult. Furthermore, once the value of $\varphi''(\sigma)$ had been established it was necessary to make one convolution to eliminate $\varphi''(\sigma)$ and another convolution with $C'_{BB}(x)$ to obtain the desired interferogram.

The procedure just outlined required at least two low resolution transformations, two convolutions and an examination of the phase plots before taking the final transformation. Therefore, an alternate method was investigated. The plan was to symmetrize the scene interferogram directly and then use the phase information to "unrectify" the final spectrum.

3.2 Spectra Rectification

As indicated by the scene phase plot (Fig. 6) a typical scene interferogram can be represented by

$$I_S(x) = \int_0^{\sigma_m} \beta(\sigma) [\; Cos2\; \sigma x + \varphi'_S(\sigma) + \varphi''_S(\sigma) + \varphi'''_S(\sigma)\;]$$

where the new term $\varphi'''(\sigma)$ has a value of either 0° or 180° depending on whether the measured radiation is positive or negative. The convolution function to symmetrize $I_S(x)$ is

$$C_S(x) = \widetilde{e}^{\;i'} [\varphi'(\sigma) + \varphi''_S(\sigma) + \varphi'''_S(\sigma)\;]$$

where $\varphi'_S(\sigma) + \varphi''_S(\sigma) + \varphi'''_S(\sigma) = \arctan S/C.$

6

The new rectified scene interferogram $I'_s(x) = I_s(x) * C_s(x)$

is plotted in Fig. 7 along with the corresponding Fourier transformation.

The transformation is essentially a plot of the absolute value of $\beta(\sigma)$

However, by examining the phase, arctan S/C, as a function of wave-

number it is possible to determine quite closely where the phase reversals

occur. The criterion used was that any phase change exceeding 20° per

wavenumber was a phase reversal. The phase information was used to

"unrectify" the spectrum plotted in Fig. 8.

A careful examination of the plotted spectra (Figs. 27, 29, 30,

and 31) reveals that at some of the phase reversal points there are errors

in amplitude. The errors are especially noticeable around 1000 cm^{-1}. The

errors are generated because the spectra are rectified by the convolution

function $C_s(x)$ before the transformation is taken. The proposed solution

was to compensate or remove $\varphi'''(\sigma)$ from the convolution function before

taking the transformation.

The procedure used was to examine the total phase function

$[\ \varphi'(\sigma) + \varphi''(\sigma) + \varphi'''(\sigma)\ ]$ wavenumber by wavenumber.

Whenever a sharp change in phase occurred, 180° was added to the total

phase. This was equivalent to generating a new function $\varphi''''(\sigma)$ nearly

equal and opposite to $\varphi'''(\sigma)$ such that

$$\varphi''''(\sigma) + \varphi'''(\sigma) = R(\sigma) \approx 0.$$

The residual function arises because $\varphi'''(\sigma)$ changes slowly due to the low

resolution, where as $\varphi''''(\sigma)$ changes instantaneously.

The new convolution function

$$C'_s(x) = e^{-i[\ \varphi'(\sigma) + \varphi''(\sigma) + R(\sigma)\ ]}$$

was convolved with $I_s(x)$ to obtain $I''_s(x) = I_s(x) * C'_s(x)$.   An

example of this interferogram and its Fourier transform are plotted in Fig. 9.

3.3 Amplitude Corrections

Ideally the convolution function should not effect the amplitude of the spectra in the region of interest. However, the experiment required that the measurements be made to a high degree of precision ±0.5%. The effect of the convolution function on the spectrum can be determined by taking its Fourier transform. The Fourier transforms of $C_{BB}(x)$, $C_s(x)$, and $C_s'(x)$ are plotted in Fig. 10. There are very pronounced dips in the amplitude of $\tilde{C}_s(x)$ as well as minor ones in $\tilde{C}_s'(x)$. Since the instrument was calibrated using the black body, it was necessary to normalize the data with respect to $\tilde{C}_{BB}(x)$.

It is interesting to note that the amplitude minima of the function $\tilde{C}_s(x)$ occur at each phase reversal of the total phase function. The computor program was written to search for the points so that the generation of the function $\varphi''''(\sigma)$ was a part of the total program.

The final complete procedure for determining the relative spectrum was as follows:

(1) Compute a low resolution spectrum using the two sided portion of the interferogram ±400 points.

(2) Use the sine and cosine components to compute the phase function,

$$\varphi'(\sigma) + \varphi''(\sigma) + \varphi'''(\sigma) = \arctan S/C.$$

(3) Compute the Fourier transform of the convolution function

$$C_s(x) = \tilde{e}^{-i[\varphi'(\sigma) + \varphi''(\sigma) + \varphi'''(\sigma)]}.$$

(4) Use the minima of (3) to generate another phase function

$$\varphi''''(\sigma) \cong -\varphi'''(\sigma)$$

(5) Generate a new convolution function

$$C_s'(x) = \tilde{e}^{-i[\varphi'(\sigma) + \varphi''(\sigma) + R(\sigma)]}.$$

(6) Convolve $I_s(x)$ and $C'_s(x)$ to obtain the final symmetric interferogram

$$I''_s(x) = \int_0^{\sigma m} B'(\sigma) \; \cos 2\pi\sigma \; x \, d\sigma$$

(7) Compute the Fourier transform of $I''_s(x)$ to obtain $B'(\sigma)$.

(8) Multiply the spectra $B'(\sigma)$ by the ratio $\widetilde{C_{BB}(x)} / \widetilde{C'_s(x)}$ to obtain $B''(\sigma)$ our closest estimate of $B(\sigma)$, the true spectra.

The final procedure required the computation of two low resolution Fourier transforms, a single convolution, and one high resolution Fourier transformation. Time wise, the convolution is the most costly step on the computer. Hence, the reduction from two to one convolution represents a considerable saving. Finally, the entire procedure was completely programmed. The resulting spectra (Fig. 11) are quite satisfactory. There is a slight decrease in signal to noise ratio near the phase reversal points due to the effect of $R(\sigma)$ on $C'_s(x)$.

4.0 Data Processing

4.1 Calibration

The final relative spectra (Fig. 9) must be converted to spectral radiance. Once the corrected relative spectra were available, the calibrations were applied to obtain the spectral radiance (Fig. 11).

The calibration information is developed from the on-board calibration black bodies and the temperature of the detector itself. The detector temperature is the reference. The instrument response to a warm target (Fig. 3) is the amplitude as a function of wavelength generated by the difference in radiance between the detector and a black body at the calibration temperature. The instrument responsivity, R, (Fig. 12) is obtained by dividing the theoretical differential radiance by the differential amplitude.

$$R_\sigma = \frac{I_\sigma \text{ target} - I_\sigma \text{detector} \atop \text{warm}}{A_\sigma \; \text{diff. target} \atop \text{warm}}$$

9

Since there are two calibration targets it is possible to calculate
an R for both the cold and the warm target.

$$R_{\sigma \text{ warm}} = I_{\sigma \text{ detector}} - I_{\sigma \text{ target cold}} \Big/ A_{\sigma \text{ cold}}$$

If it is assumed that R_σ cold and R_σ warm are equal, then

$$(1) \quad R_\sigma = I_{\sigma \text{ warm target}} - I_{\sigma \text{ cold target}} \Big/ A_{\sigma \text{ cold}} + A_{\sigma \text{ warm}}$$

The responsivity calculated using this relation is given in Fig. 12.

The spectral radiance for a given wave number is given by

$$(2) \quad I_\sigma \text{ unknown} = I_\sigma \text{ det} + R_\sigma A \text{ unknown}$$

A typical plot is shown in Fig. 11.

4.2 Noise Evaluation

The primary objective for making measurements of I_σ are for
the calculations of temperature profiles. It is generally agreed that mean-[5,6,7]
ingful temperature profiles can be obtained if I_σ can be measured to an
accuracy of $0.5 \text{ erg/cm}^2 \cdot \text{ster} \cdot \text{sec} \cdot \text{cm}^{-1}$ averaged over 5 cm^{-1}.

In order to achieve the required measurement accuracy very
careful attention must be paid to the possible errors. It can be seen from
equations (1) and (2) that a total of 6 separate measurements are involved
in the determination of I_σ unknown.

There are two types of measurements. The values of $I_{\sigma \text{ warm}}$,
$I_{\sigma \text{ cold}}$ and $I_{\sigma \text{ detector}}$ are determined by the temperature measurements.
Any error in the measurements represents a systematic error which cannot
be reduced by multiple scans of the same scene.

The errors in the measurements of $A_{\sigma \text{ warm}}$, $A_{\sigma \text{ cold}}$, and
$A_{\sigma \text{ unknown}}$ are the result of noise which can be reduced by multiple scans
of the same scene. The random errors in the A_σ measurements were
determined by calculating the spectral radiance of an unknown black body
target in both low and high resolution (Fig. 13). The standard deviation of

one spectra from the other is a measure of the noise in the spectrum. The total random noise is contributed by $A_{\sigma \ warm}$ and $A_{\sigma \ cold}$ in calculating values of R_{σ} as well as by the noise in $A_{\sigma \ unknown}$.

The average standard deviation (Fig. 13) was 0.5 erg units for an interval of 13.5 cm^{-1}. The equivalent deviation for 5 cm^{-1} interval is 0.85 erg units. The value is greater than the desired specification and in order to obtain useable data, averaging is required. The experimental instrument was set to average four scenes. The random deviation for an average of four scenes is 0.43 ergs units.

The best possible accuracy for making in-flight temperature measurements of the calibration black bodies is approximately 0.1° C. At a temperature of 273° K this is equivalent to 0.1 erg units. All the I errors enter in the same way so that the probable systematic error is 0.17 $ergs/cm^{2} \cdot sr \cdot sec \ cm^{-1}$.

$$(3) \qquad \xi_{total} = \sqrt{\xi_{A}^{2} + \xi_{I}^{2}}$$

For temperature variation $\pm 0.1^{\circ}$ K $\quad \xi_{total} = \sqrt{\xi_{A}^{2} + \xi_{I \ 0.1}^{2}} = \sqrt{.43^{+2} + .17^{+2}}$

0.45 erg units.

For a temperature variation of $\pm 0.2^{\circ}$ K, $\xi_{total} = \sqrt{.43^{+2} + .34^{+2}} = 0.54$ erg units.

Hence, due to the random error it is necessary that the calibration and detector temperatures be measured to an accuracy of 0.1° K. Such accuracy was the design goal and was achieved on the original flight. However, due to circuit failures in the housekeeping channels the temperature errors on the last flight were in excess of 0.5° K.

5.0 Instrument Description

The basic instrument was described in a previous report and the specifications are given in Table 1. The instrument is basically a Michelson interferometer (Fig. 14). The light paths are shown on the figure. The position of the moving mirror is measured by an essentially monochromatic line furnished by the neon bulb and isolated by a narrow band filter. The neon signal is detected by the photo-diode as a slightly modulated sine wave (Fig. 4). The sine wave activates a trigger circuit and divider to furnish a digitizing pulse every second wave. The amplitude of the infrared signal detected by the thermistor balometer is transmitted in serial digital form (Fig. 16) to the telemetry channel.

The physical modifications to the original instrument were a new drive unit, a new narrow band interference filter in the neon channel and the rewiring of the logic circuit. The new drive unit (Fig. 17) was made with longer parallel springs (85 cm) and a greater distance between springs (90 cm). The housing was made of stainless steel **rather** than aluminum in order to minimize temperature distorting effects. The drive modification was required in order to reduce the tilting of the mirror. In the original instrument the tilt could be divided between the two sides and the permissable total tilt was twice as large. The total angular displacement was less than 2 arc seconds.

The new narrow band filter was centered at 0.7032μ instead of 0.5852μ. Although the new line was less prominant visually, the detector was more sensitive. The signal to noise improvement was almost a factor of two. As a result of using the longer wavelength it was necessary to change the logic to produce fewer records per scan. The last 64 words in each scan were used

to read out the housekeeping channels through the MOS-FET commutater. During the flight preparations three of the MOS-FETS unknowingly failed and put an unknown resistance load in parallel with the monitored signals. A first order correction was made by solving for the resistance using a prior knowledge of several of the monitored voltages. The accuracy of the correction was limited to about 5% and accounts for the large uncertainty in the values of I .

5.1 Instrument Housing

The instrument housing (Fig. 15 & 18) was designed to provide a stable environment for the instrument during the flight. The melting ice provided the reference and the nitrogen environment purged the water vapor from the system. The liquid nitrogen was stored in a 10 liter flask mounted adjacent to the optics.

The liquid nitrogen flowed from the flask through 12 inches of 1/4 inch pipe and a choke valve to the cold black body. Foam insulation was used around the pipe and valve. Although the system was checked several times in environmental chambers, it failed to function properly during the balloon flight. The explanation for the failure was that the foam insulation was not adequate to provide a stable environment. During the previous flight a smaller 3 liter flask was used and the foam insulated section of line was about 4 inches long. The shorter section of line minimized the thermal fluctuations and allowed a stable flow pattern to be maintained.

The electronics (Fig. 19 and 20) was contained in a package 8"x8"x16". All the circuits were solid state including mostly integrated circuits but experimental cards were used throughout the package. The electronics package of the satellite version of the same instrument was reduced to approximately a 6 inch cube.

5.2 Auxilliary Modification

An auxilliary modification of the instrument operation consisted of a moveable mirror mounted below the instrument (Fig. 21). There was a hinge on one side of the mirror and the other side was positioned by means of ball detents. A double chain drive moved the mirror to the desired location.

The mirror was positioned by commands from a programmer which also controlled the start time of each interferogram. The program repeated itself after a sequence of 16 interferogram scans. Four scans were made of the scene below the gondola. Two scans were made observing the cold black body and two observing the warm black body. The auxilliary mirror moved into a 45° position and two scans were made observing the horizon, followed by two scans at 22° and two at 44° above the horizon. During the last two scans the mirror was positioned horizontally and the instrument observed the bottom of the gondola. The bottom was painted with 3-M Black Velvet and the temperature was monitored by a thermistor.

The programmer (Fig. 22) was a solid state timing device originally designed to simulate spacecraft signals required by the satellite instrument flown on the same gondola. The basic timer was a 200 KC crystal oscillator followed by a series of count down circuits to 1/512 second. By the use of the proper coincident gates it was possible to generate pulses of any desired duration to occur at any time during the 512 second period. The programmer was constructed using standard circuit packages purchased from Radiation, Inc.

5.3 Gondola Flight Path

The balloon was launched from Rapid City, S. D. on November 20, 1968 at 1308 Z or 0608 MST. The general direction of the flight was southward and the flight was terminated by command at 2031 Z and impacted near Kimball, Nebraska at 2111 Z. The trajectory is shown in Fig. 23. From the times given on the trajectory the location of the balloon for any of the data sets reported can be determined.

14

6.0 Measurements

The in-flight measurements as indicated in the last section consisted of calibrations, earth scenes, and horizon observations. The data was recorded from 14:20 Z to 19:14 Z. The starting time was set by the opening of the instrument door about 20 minutes before reaching float altitude. The recording was arranged so that in a given 21:20 period two sets of 16 interferograms were recorded and in the alternating 21:20 period one set was recorded. There was a time sharing of the telemetry channel with the satellite instrument and the blank periods were required for rewinding the tape and setting up the tape recorder.

The data set which was investigated most completely was recorded at 14:30 Z shortly after the balloon reached float altitude. The measured spectral radiances are given in (Fig. 24-26). Scene data looking downward was reduced for 6 sequences between 15:04 Z and 19:14 Z. The last set was obtained from the down range station which accounts for the time gap between the last two sets. The average scene spectral radiance for each set is plotted in (Figs. 27-32). The associated photograph is given with each data set.

6.1 The Black Body Data

The data acquisition system was designed to provide calibration with each set. However, much of the calibration data was not used because of the drift in the temperature of the cold black body. As noted previously, the liquid nitrogen control system failed to maintain a minimum flow and the cold black body warmed up during the flight. The cooling effect of the tropopause helped to keep the cold black body at the relatively constant temperature during three data sets recorded over a period of one hour. The data from the three sets was averaged and used for calibration.

15

Typical black body spectral radiances measured using the first calibrations are plotted in (Figs. 33 and 34). Included in the same plot is the theoretical spectral radiance corresponding to the measured temperature. The deviation of the measurements from the theoretical values indicates an error in the calibration.

An examination of the black body relative amplitude plots indicated a difference in responsivity between the warm and cold targets. The conclusion arrived at, was that the error resulted from a malfunction in the gain changing amplifier. Whenever the amplifier gain decreased a voltage off-set appeared at the amplifier input. The off-set was compensated in the computer program. However, it is possible that the off-set produced an uncompensated non-linearity. The non-linearity would effect one polarity of the signal and not the other. Hence, a new calibration using the warm black body temperatures only was applied. The warm black body fits the theoretical data, but the cold does not.

6.2 Scene Data

The scene data is presented in Figs. 27 through 32. The notable change in the spectral radiance occurs in the window region. The ground tem perature gradually increased during the day producing the noted results. The 15μ band equivalent temperatures seemed to increase slightly during the day and the 6.3μ water vapor band exhibited very little change.

The spectra shown in Figs. 29 to 31 were reduced by using a single convolution function which produced errors associated with the spectrum rectification. The error is very apparent around 1000 cm^{-1}. The spectra shown in Figs. 28 and 32 were reduced by our most sophisticated technique. These are the best spectra obtainable by the one-sided interferogram method. There is a 70%-80% decrease in the signal to noise ratio near the signal reversal points, but otherwise the data is quite satisfactory.

6.3 Atmospheric Data

The atmospheric data (Fig. 24 to 26) is that obtained by observing horizontally and at 22° and 44° above the horizon. The original objective in obtaining the data was to compute the CO_2 concentration at balloon flight altitudes. However, due to the uncertainty of the calibrations, it was decided not to proceed with the data reduction effort. Qualitatively the data is interesting in that the CO_2 radiance is the dominant feature. The effect of ozone and water vapor are both very small.

7.0 Data Evaluation

7.1 Temperature Inversions

The primary purpose in obtaining the data was to make temperature inversions. An inversion calculated from the data plotted in Fig. 32 is shown in Fig. 37. The plotted inversion is quite good and agrees very well with the radiosonde data. The large standard deviations associated with the black body and detector temperature measurements could shift the entire curve through the range indicated. However, the fact that the shape of the curve is basically correct indicates that the random noise is within acceptable limits.

7.2 Qualitative Observation

The principal water vapor lines near 1650 cm^{-1} and 600 cm^{-1} change very little during the course of the flight. However, the very weak lines in the window area do change and become much more prominent as the flight progresses. The change in the weak lines are an indication of the water vapor near the surface. It seems that by the proper selection of individual lines, a knowledge of their transmissivity, and a knowledge of the temperature distribution that the water vapor distribution can be determined. A study would have to be made to determine the optimum spectral resolution required.

17

Ozone, another variable gas, contributes to the heat transfer in the atmosphere. Satellite measurements of both the quantity and distribution of ozone would be extremely desireable. Projects to develop mathematical techniques to deduce the distribution from the spectral radiance are now underway. When some of the problems associated with the inversion are solved, the present data should be useful. One of the principal problems associated with ozone is to establish the correct transmissivity.

Restrahlen Bands

The investigation of the possibility of detecting restrahlen bands due to surface minerals was another objective of the flights. A comparison of spectra (Fig. 38) obtained from the May 1966 flight over grass land and the November 1968 flight over barren soil indicates that the restrahlen effects are virtually non-existent due to the presence of ozone.

8.0 Conclusion

Although it is possible to essentially double the resolution of a Fourier transform spectrometer by operating in a one-sided mode, it is our conclusion that the method should be used only after careful consideration. The increased computing time and the increased programming complexities are definite disadvantages.

The increased resolution from 5 cm^{-1} to 2.5 cm^{-1} is useful for the study of weak water vapor bands, but of no particular advantage in performing the temperature inversions. It is quite probable that the increased resolution will be an aid in measuring the ozone distribution, but not enough work has been done in this area to make a definitive statement.

The data obtained from atmospheric paths above the horizon is qualitatively interesting. If the instrument performed to specifications, the data would be useful for measuring CO_2 concentrations. It is suggested that the portion of the experiment be repeated on future flights.

The experimental one-sided interferometer was essentially destroyed on the last flight. However, the prototype satellite interferometer flown at the same time survived. It is suggested that this instrument, two-sided 5 cm^{-1} resolution, be flown with an external viewing mirror to observe both the ground and the atmosphere above the balloon. The instrument would probably be flown with other advanced meteorological excitation instruments such as the J. P. L. 4.3μ spectrometer and the M. I. T. microwave radiometer.

References

1. Chaney, L. W., Earth radiation measurements by interferometer from a high altitude balloon. Proceedings of the Third Symposium on Remote Sensing of the Environment, Ann Arbor, Michigan, 1964.

2. Chaney, L. W., Drayson, S. R., and C. Young, Fourier transform spectrometer — Radiative measurements and temperature inversion. Applied Optics $\underline{6}$, 1967.

3. Hanel, R. A. and Conrath, B. J., Interferometer experiments on Nimbus III: Preliminary results. Science Vol. $\underline{165}$, No. 3899, p. 1248. 1969.

4. Forman, M. L., W. H. Steel and G. A. Vanasse, Correction of asymmetric interferograms obtained in fourier spectroscopy, J. Opt. Soc. Am. $\underline{56}$, 59, 1966.

5. Forman, M. L., W. H. Steel and G. A. Vanasse, Non-linear phase corrections of interferograms obtained in fourier spectroscopy, AFCRL 65-518, 1965.

6. Vanasse, G. A. and Sakai, H., Fourier spectroscopy, Progress in Optics Vol. VI, p. 261, North Holland Publishing Co., 1967.

7. Kaplan, L. D. Inference of atmospheric structure from remote radiation measurements, J. Opt. Soc. Am., $\underline{49}$, pp. 1004, 1959.

8. Wark, D. Q., On indirect temperature soundings of the stratosphere from satellites, J. Geophys. Res. $\underline{66}$, p. 77, 1961.

9. Drayson, S. R., Errors in atmospheric temperature structure solutions from remote radiometric measurements. U. of M. Tech. Report 05863-4-T, 1963.

10. Drayson, S. R., Atmospheric slant path transmission in the 15 CO_2 band, U. of M. Tech. Report, 05863-6-T, 1964.

TABLE I

Instrument Specifications

Spectral range: 2000 - 500 cm^{-1} (5-20)

Spectral resolution: 2.5 cm^{-1} from 500-1000 cm^{-1} decreasing to 5 cm^{-1} at 2000 cm^{-1}

Optical path displacement: 0.4 cm

Diameter of effective aperature: 3.6 cm

Detector: Thermistor Bolometer in conical light pipe

Detector time constant: $1.2 \cdot 10^{-3}$ sec.

Detector frequency band: 20-80 cps.

Data scan time: 11 seconds

Sampling: every second fringe of 1032 A^o monochromatic neon line

Sampling rate: 260 words per second

Words per interferogram: 2960

Field of view: 1.57×10^{-2} ster (approx. 8°)

Peak signal to noise: 1500

Reference temperature: $273^o K$

$$I(x) = \int_{0}^{\sigma_m} \beta(\sigma) \cos\left[2\pi\sigma x + \phi(\sigma)\right] d\sigma$$
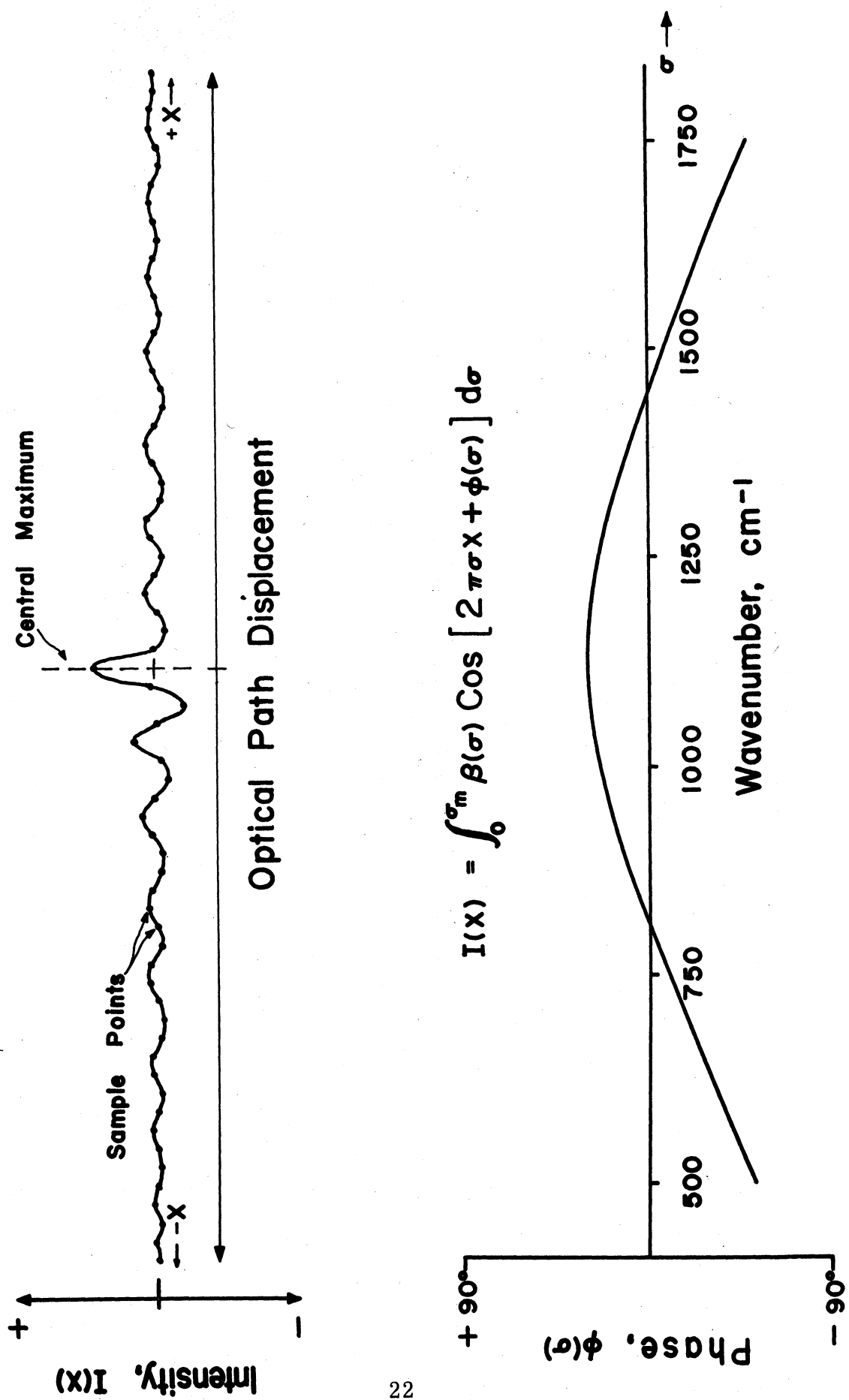
Figure 1. A typical blackbody interferogram ideally sampled and the corresponding phase function.

$$I(x) = \int_0^{\sigma_m} \beta(\sigma) \cos 2\pi\sigma x\, d\sigma$$
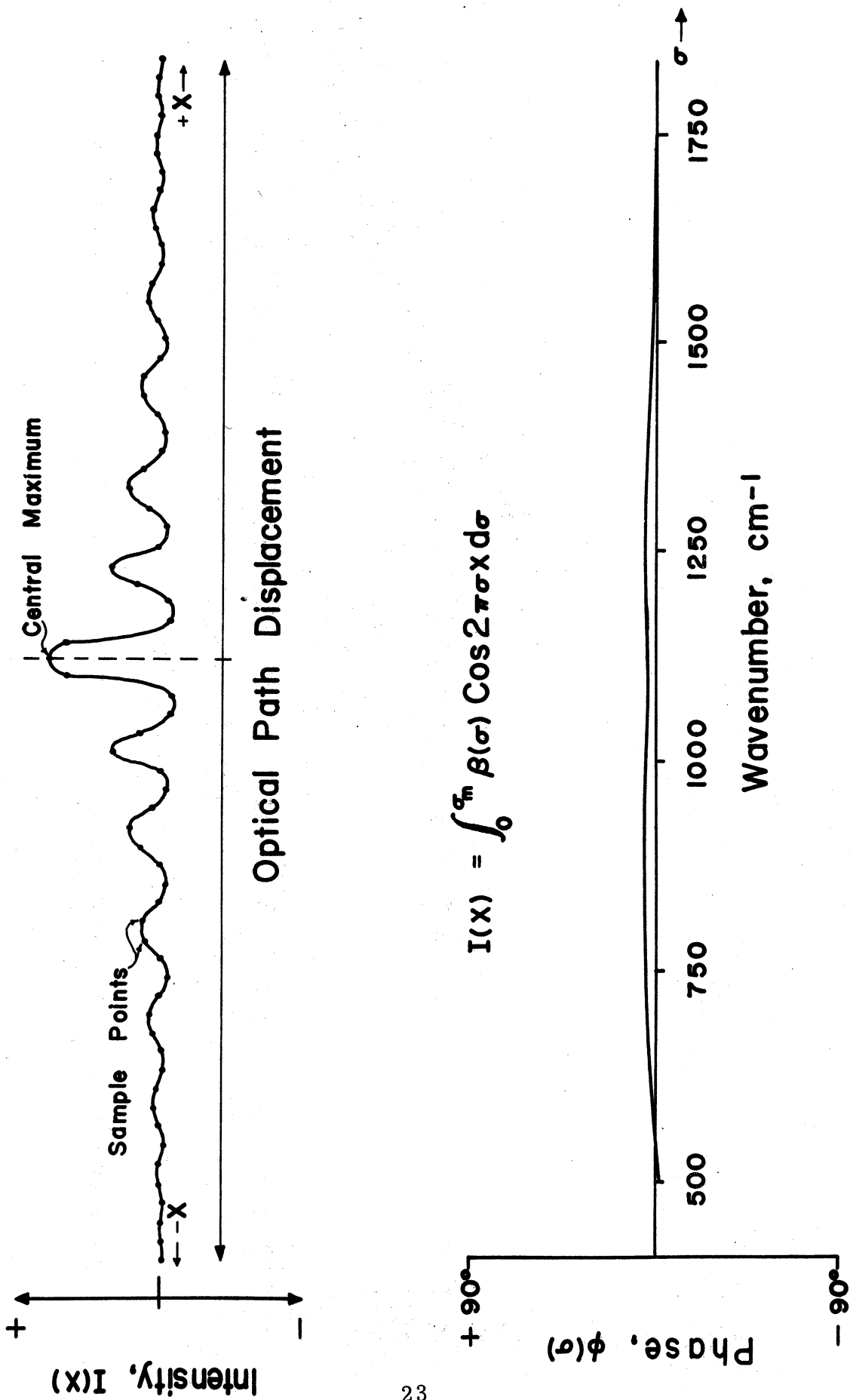
Figure 2. An ideal interferogram ideally sampled and the residual phase function.

23
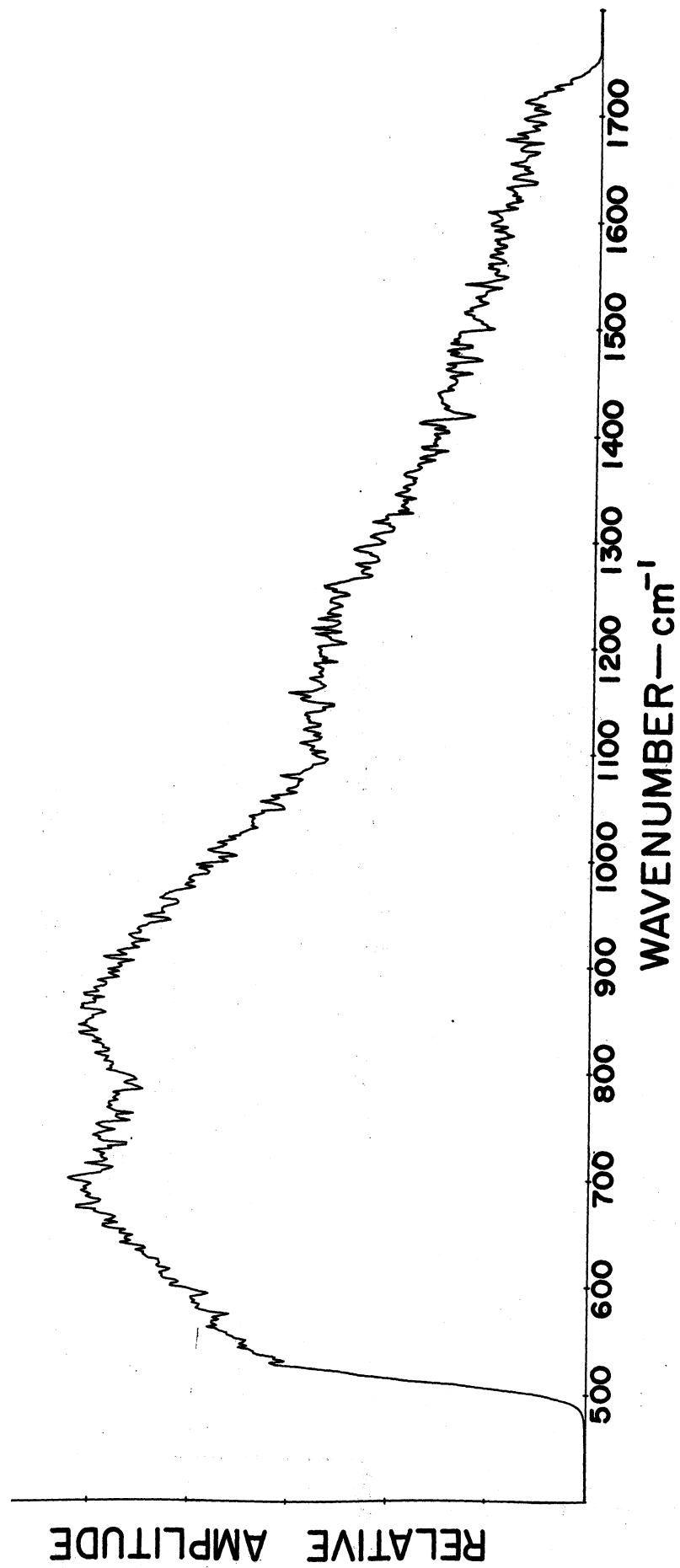
Figure 3.   Fourier transform of a symmetrical interferogram derived from a warm blackbody observation.
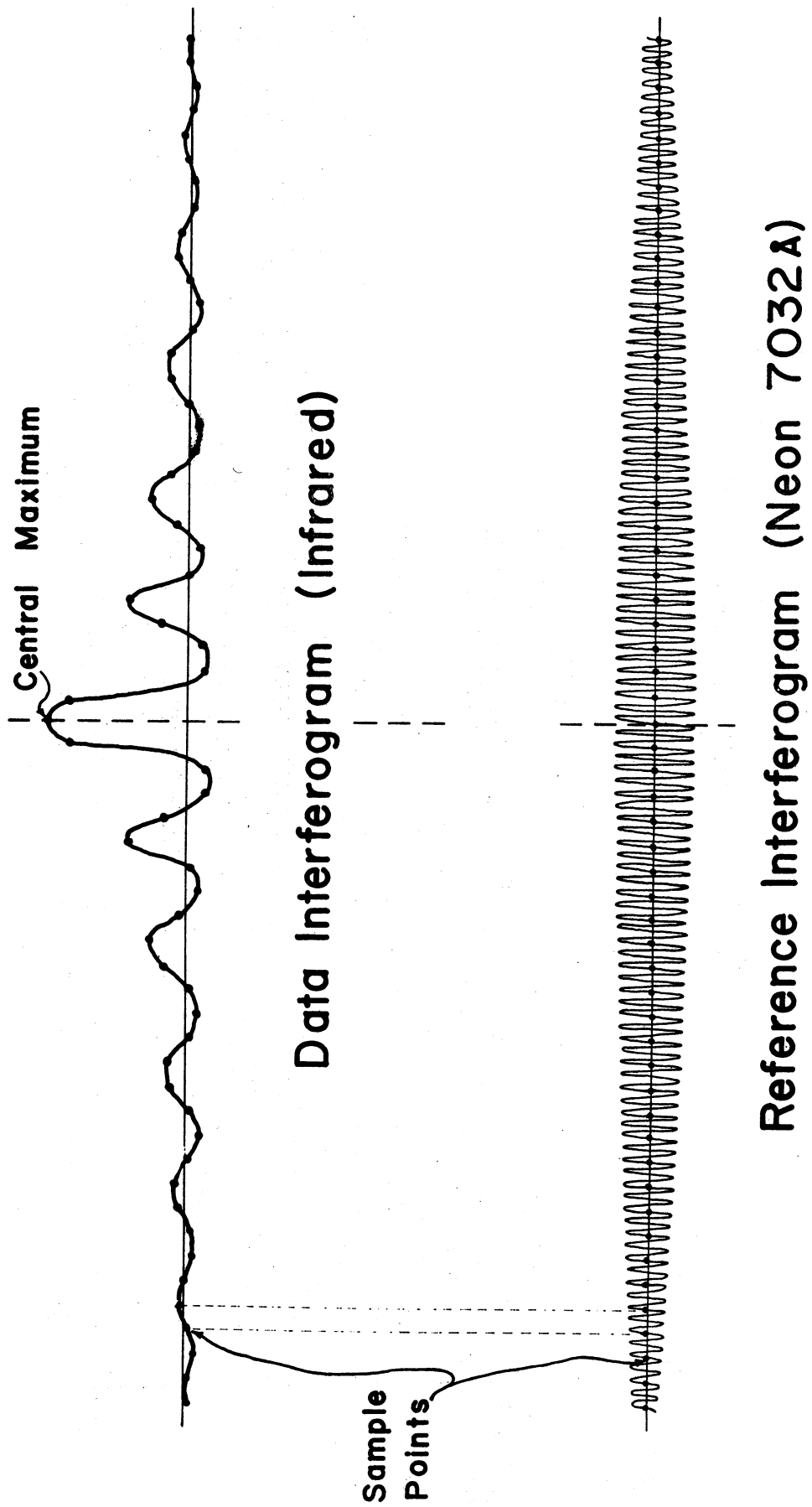
Figure 4. Comparison of infrared and neon interferograms.

Central Maximum

Data Interferogram (Infrared)

Reference Interferogram (Neon 7032Å)

Sample
Points

$$I(x) = \int_{0}^{\sigma_m} \beta(\sigma) \cos\left[2\pi\sigma x + \phi'(\sigma) + \phi''(\sigma)\right] d\sigma$$

$$\phi''(\sigma) = -2\pi\sigma\xi$$
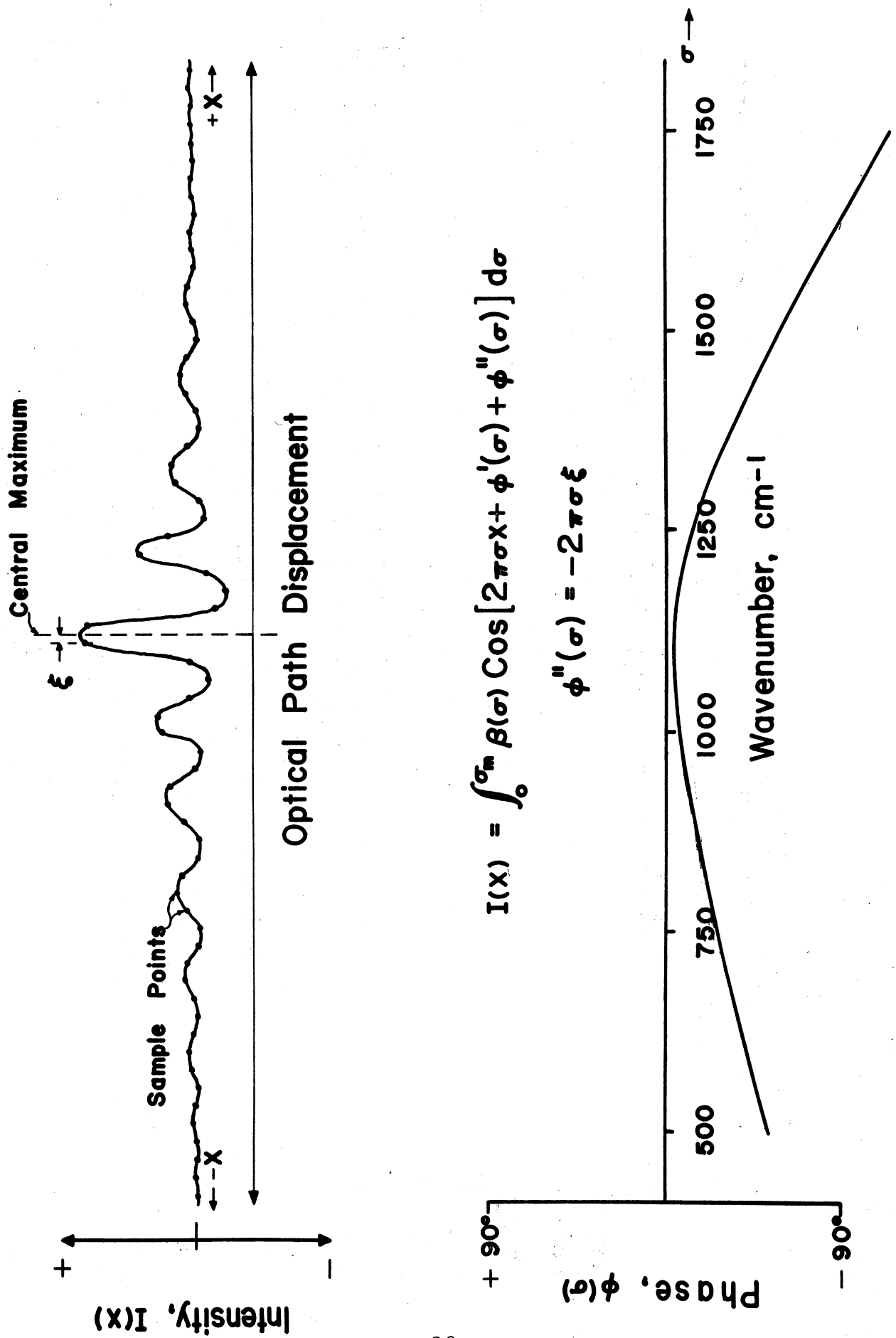
Figure 5. A typical blackbody interferogram typically sampled and the corresponding phase function.
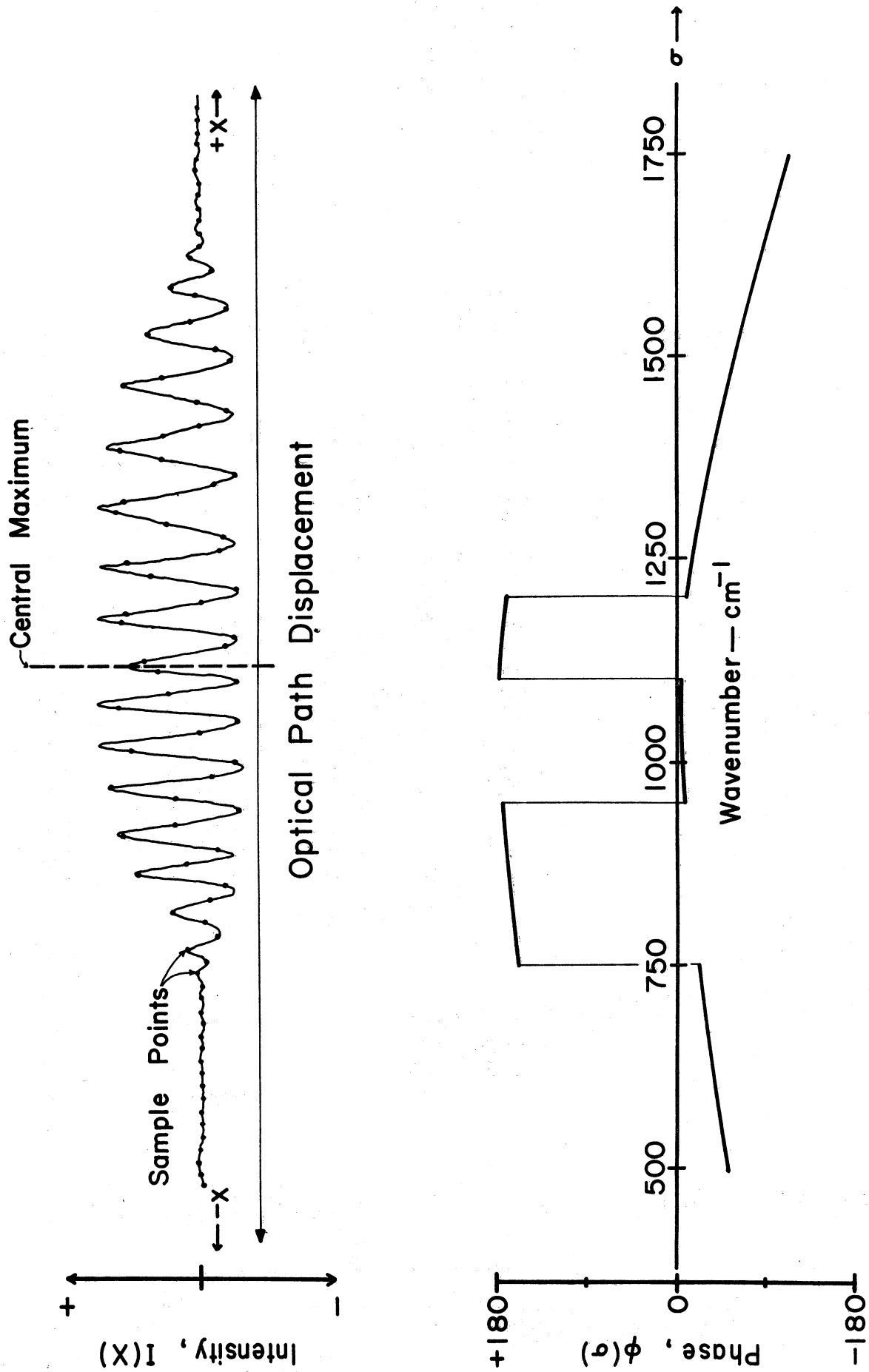
$$I(x) = \int_0^{\sigma_m} \beta(\sigma) \cos[2\pi\sigma x + \phi'(\sigma) + \phi''(\sigma) + \phi'''(\sigma)]\, d\sigma$$

Figure 6. A typical scene interferogram typically sampled and the corresponding phase function.

27
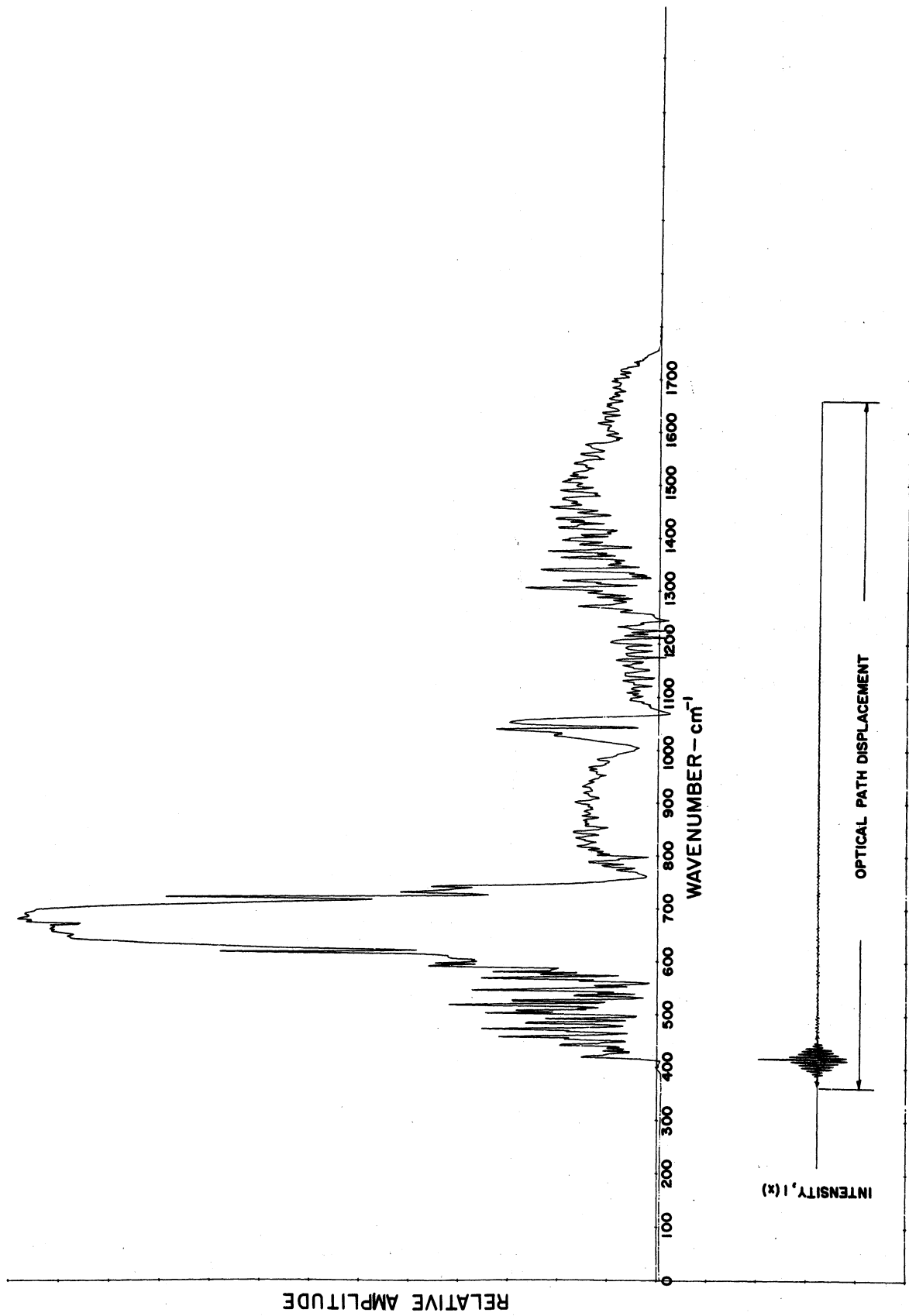
Figure 7. A "rectified" scene interferogram and its final transform.
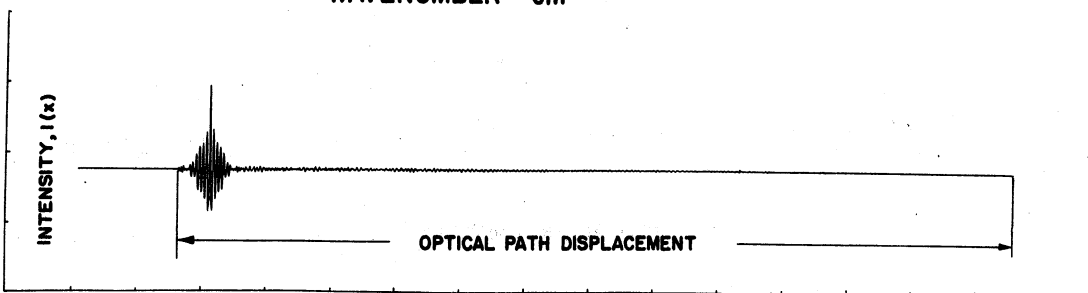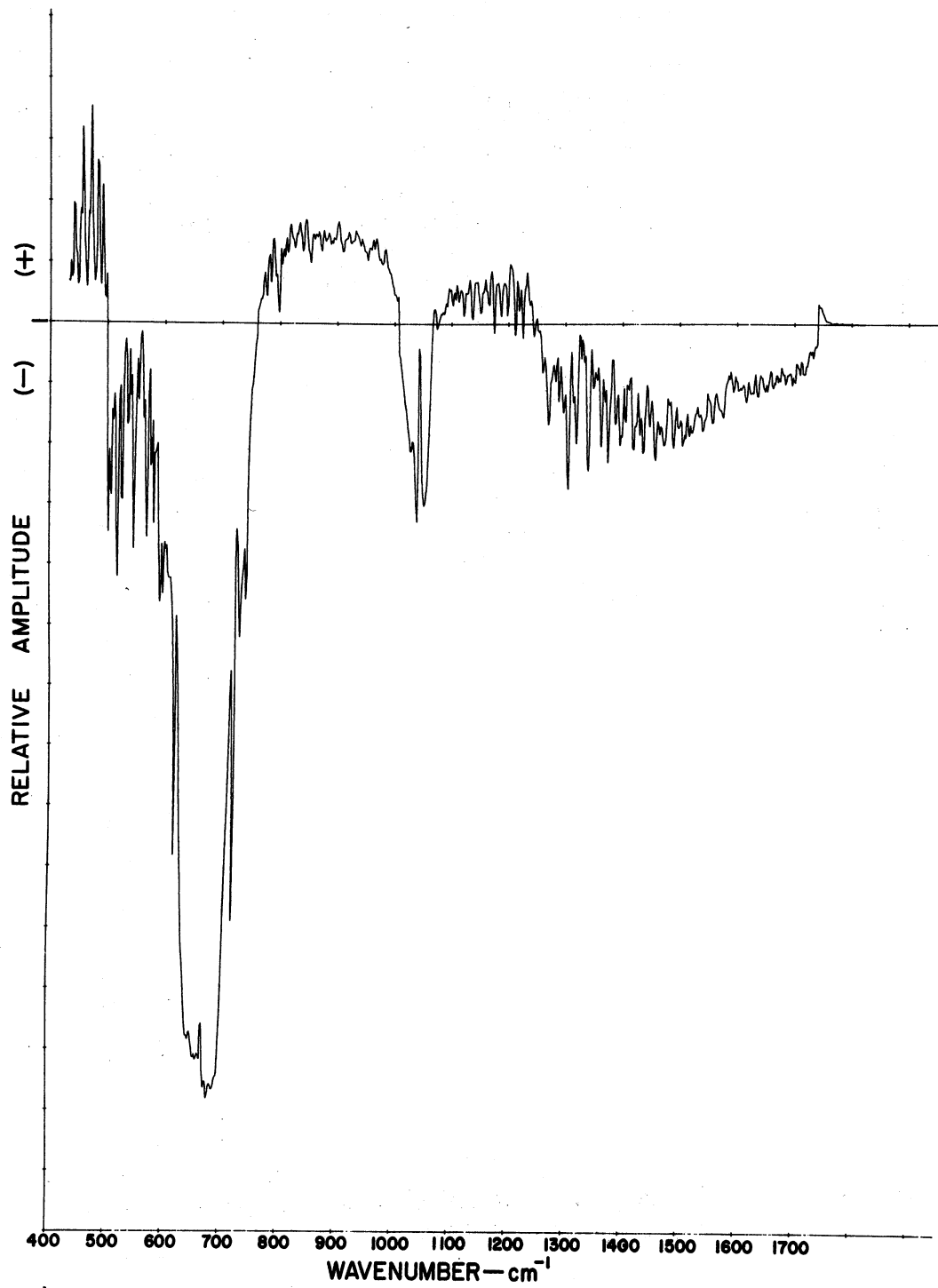
Figure 8. A scene spectrum "unrectified"
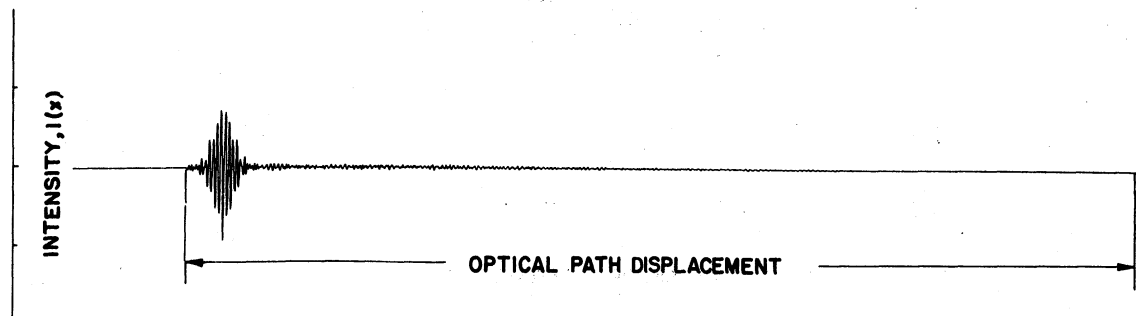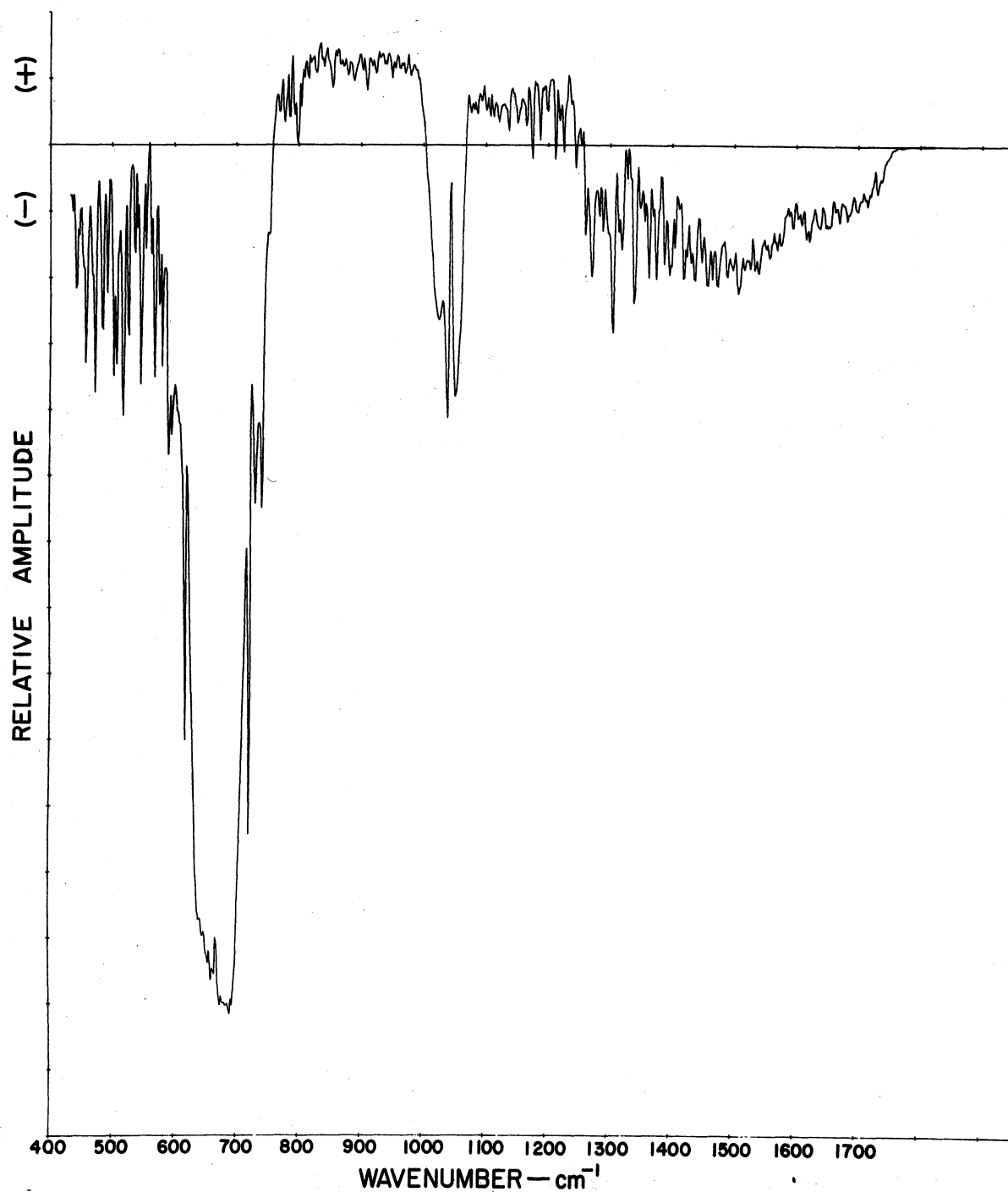
Figure 9. A fully corrected scene interferogram and its transform.

30
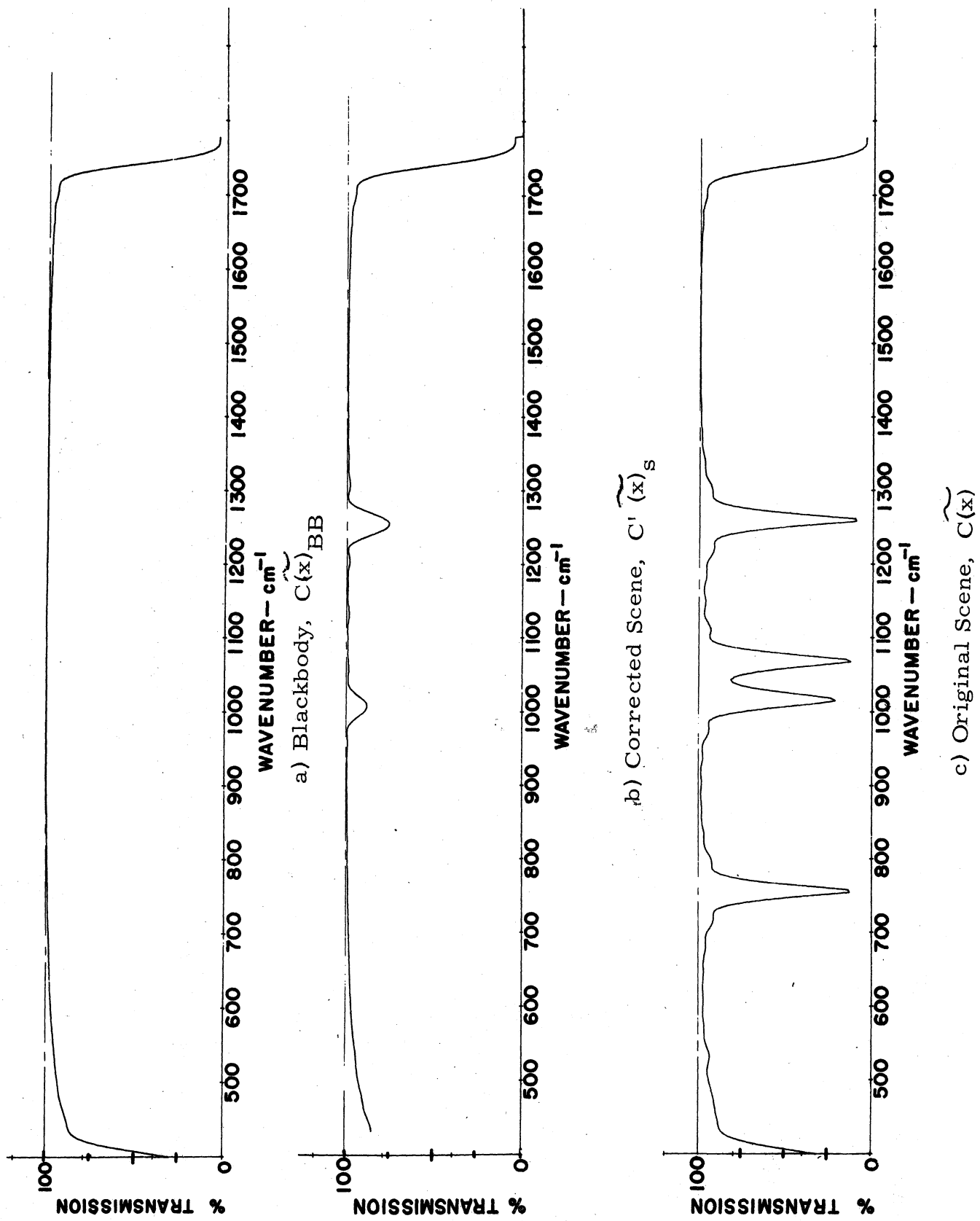
Figure 10. A comparison of Convolution Functions
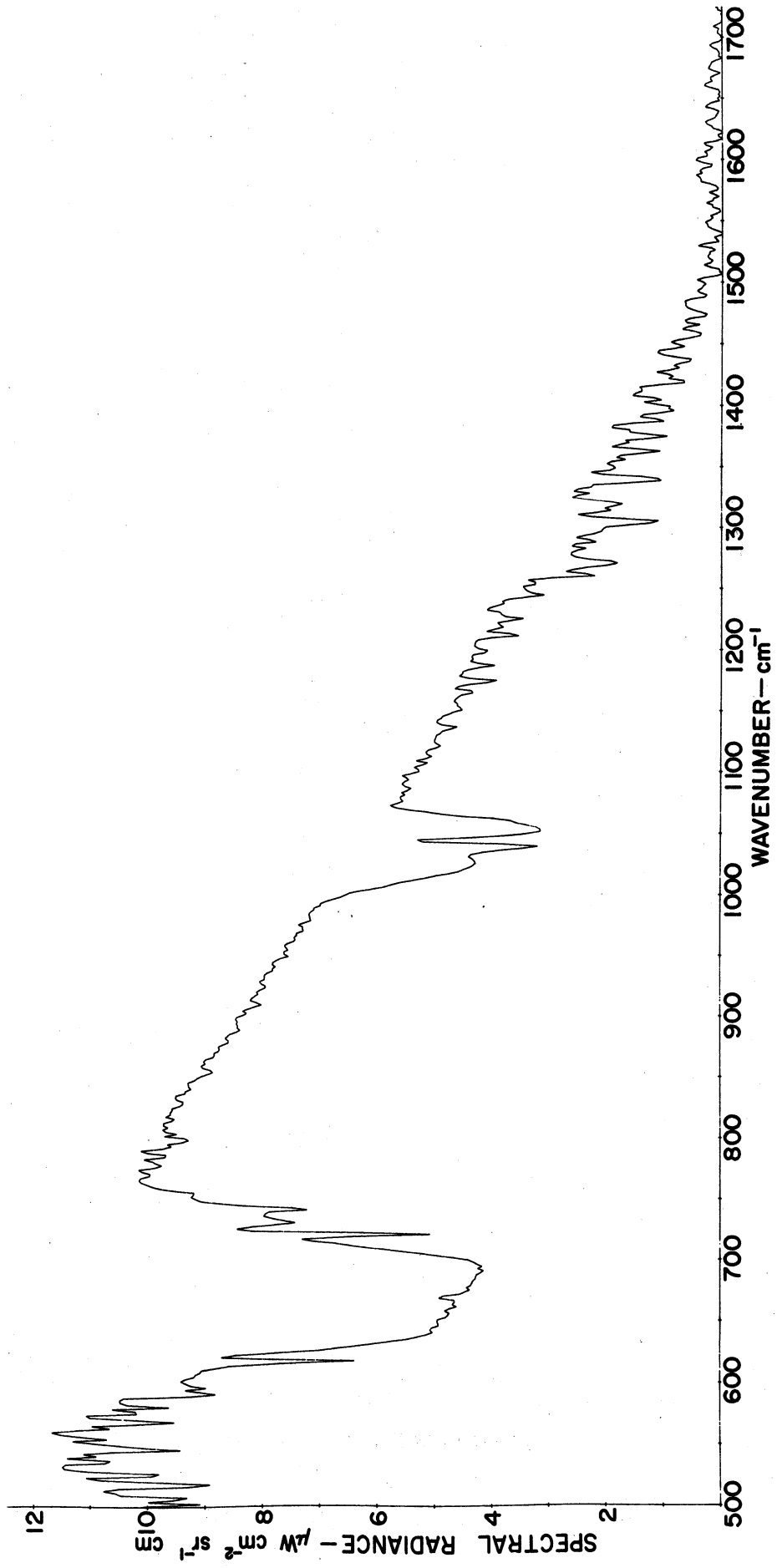
Figure 11. Final Scene Spectrum After All Corrections and Calibrations
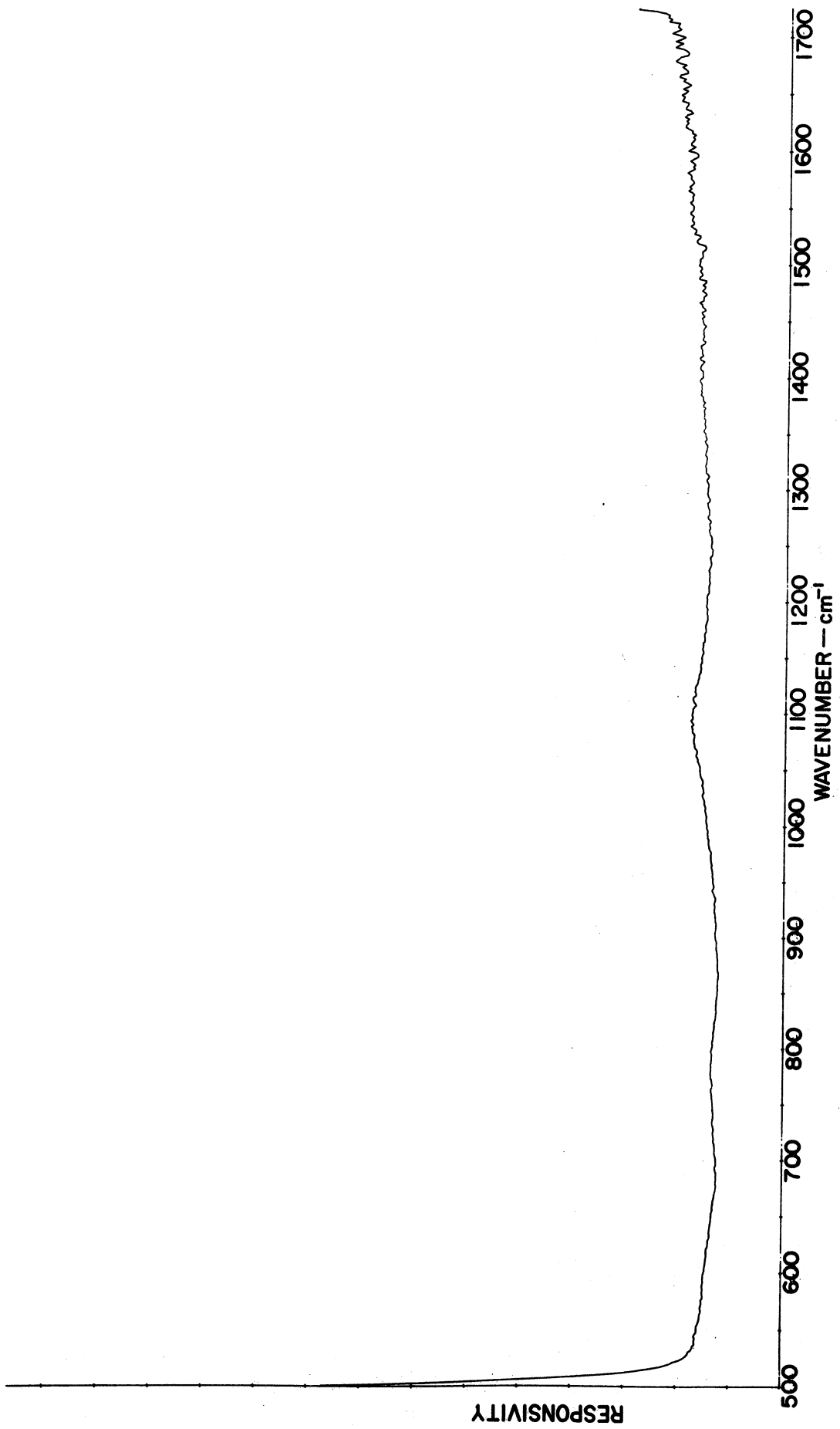
Figure 12. Instrument responsivity: Differential radiance/Differential Instrument Output

33
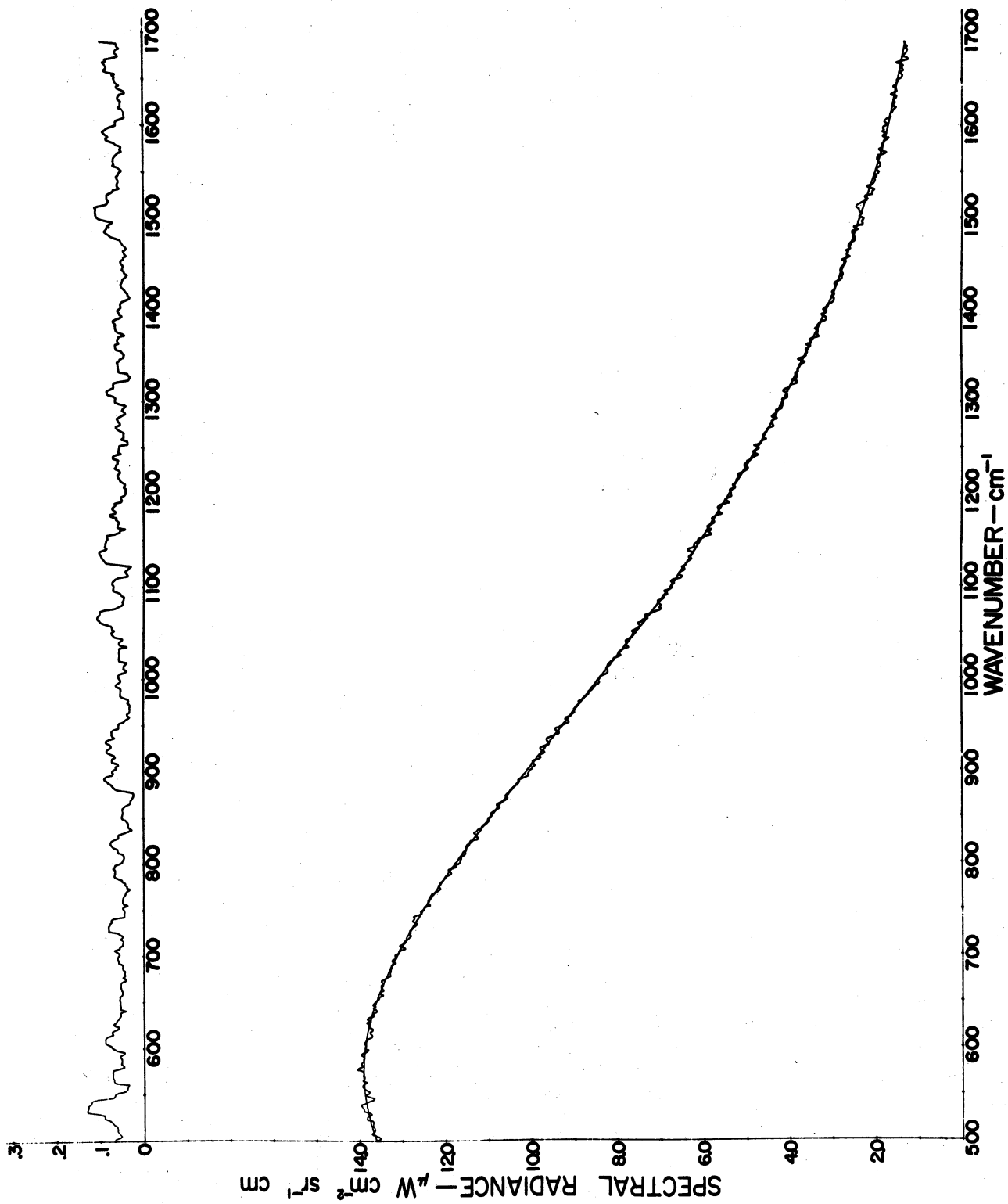
Figure 13. A high and low resolution spectrum of the same blackbody and the corresponding standard deviation.

34
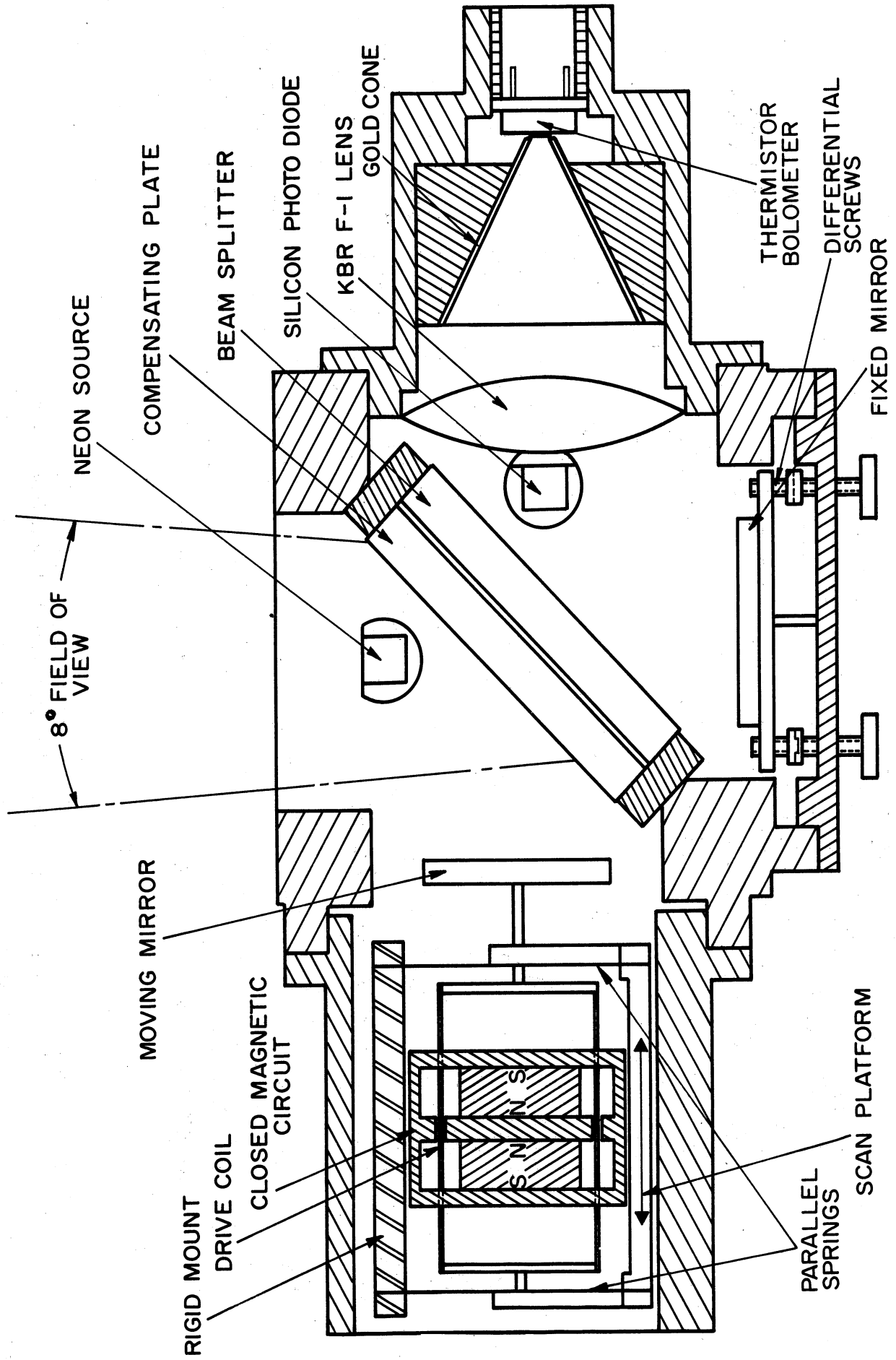
Figure 14. **OPTICAL HEAD LAYOUT**

NEON SOURCE

COMPENSATING PLATE

BEAM SPLITTER

SILICON PHOTO DIODE

KBR F-l LENS

GOLD CONE

THERMISTOR BOLOMETER

DIFFERENTIAL SCREWS

FIXED MIRROR

8° FIELD OF VIEW

MOVING MIRROR

RIGID MOUNT

DRIVE COIL

CLOSED MAGNETIC CIRCUIT

S N N S

S N N S

PARALLEL SPRINGS

SCAN PLATFORM

URATHANE INSULATION

WARM BLACK BODY

BASEPLATE— VACUUM TIGHT & WATER FILLED

LIQ. N₂

N₂ GAS

COLD BLACK BODY

RADIATION PORT

DOOR

SHOCK MOUNTS

GONDOLA PLATFORM

Figure 15. Interferometer in balloon flight package.

36
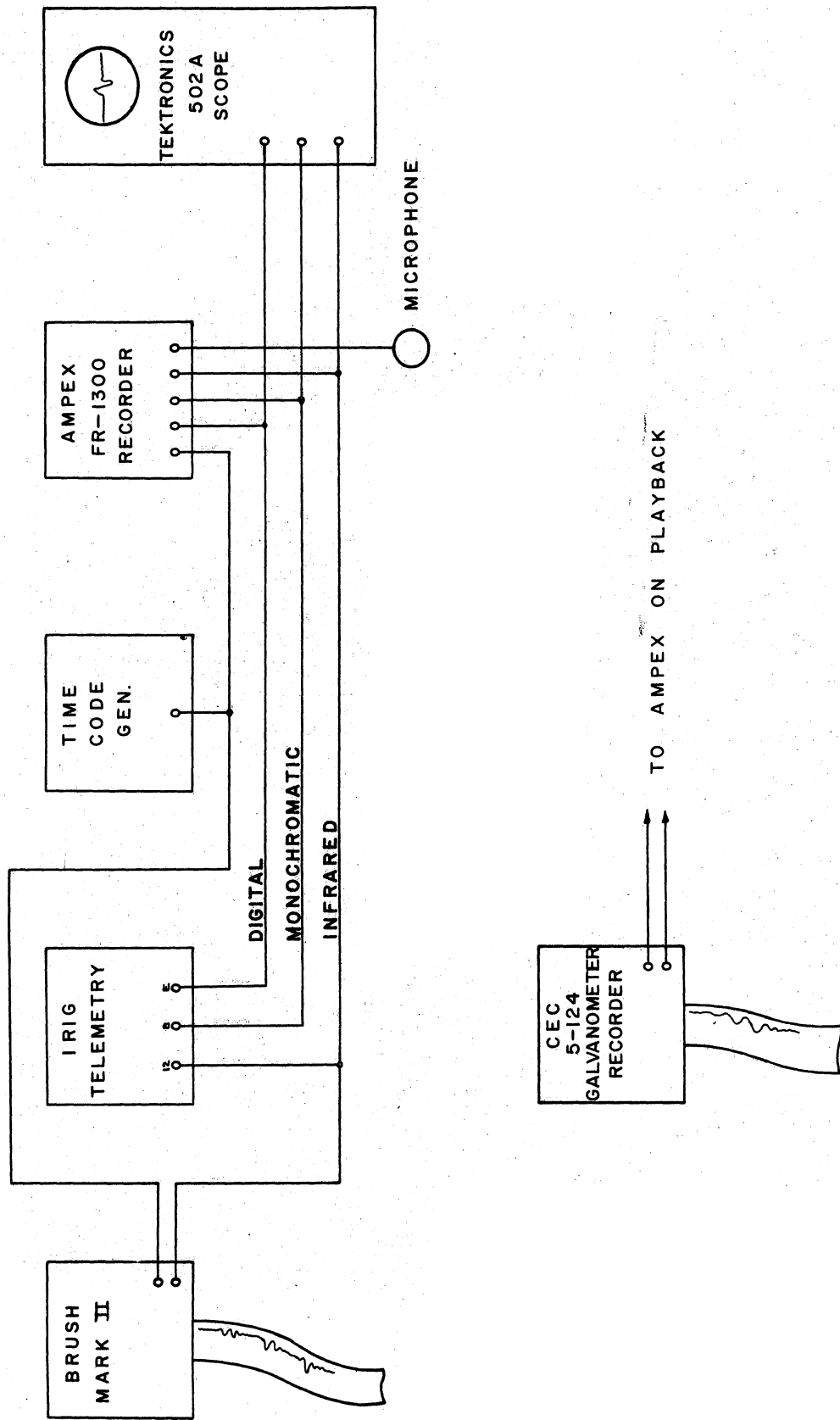
Figure 16. A typical serial digital word.
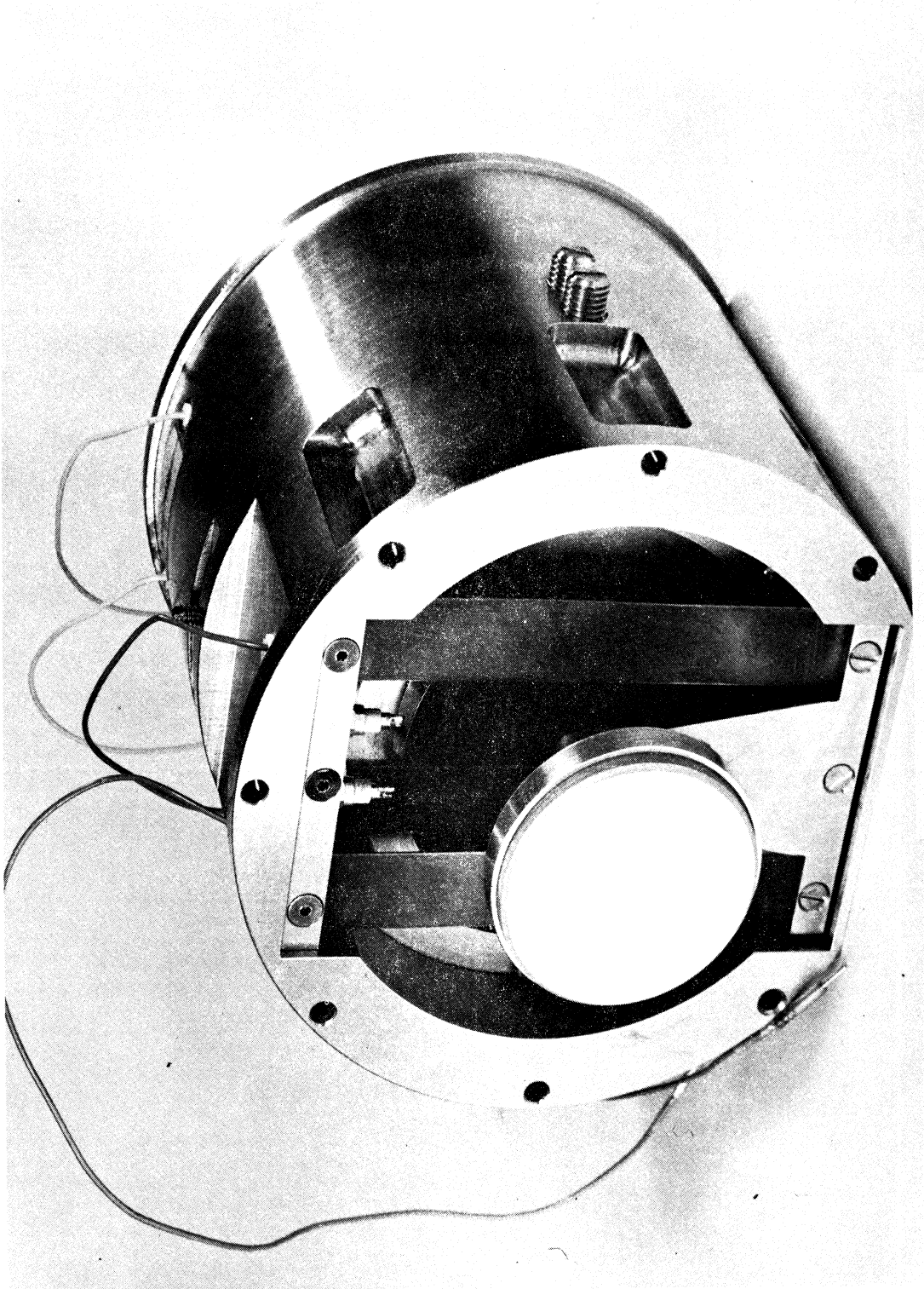
Figure 17. Michelson Mirror Drive
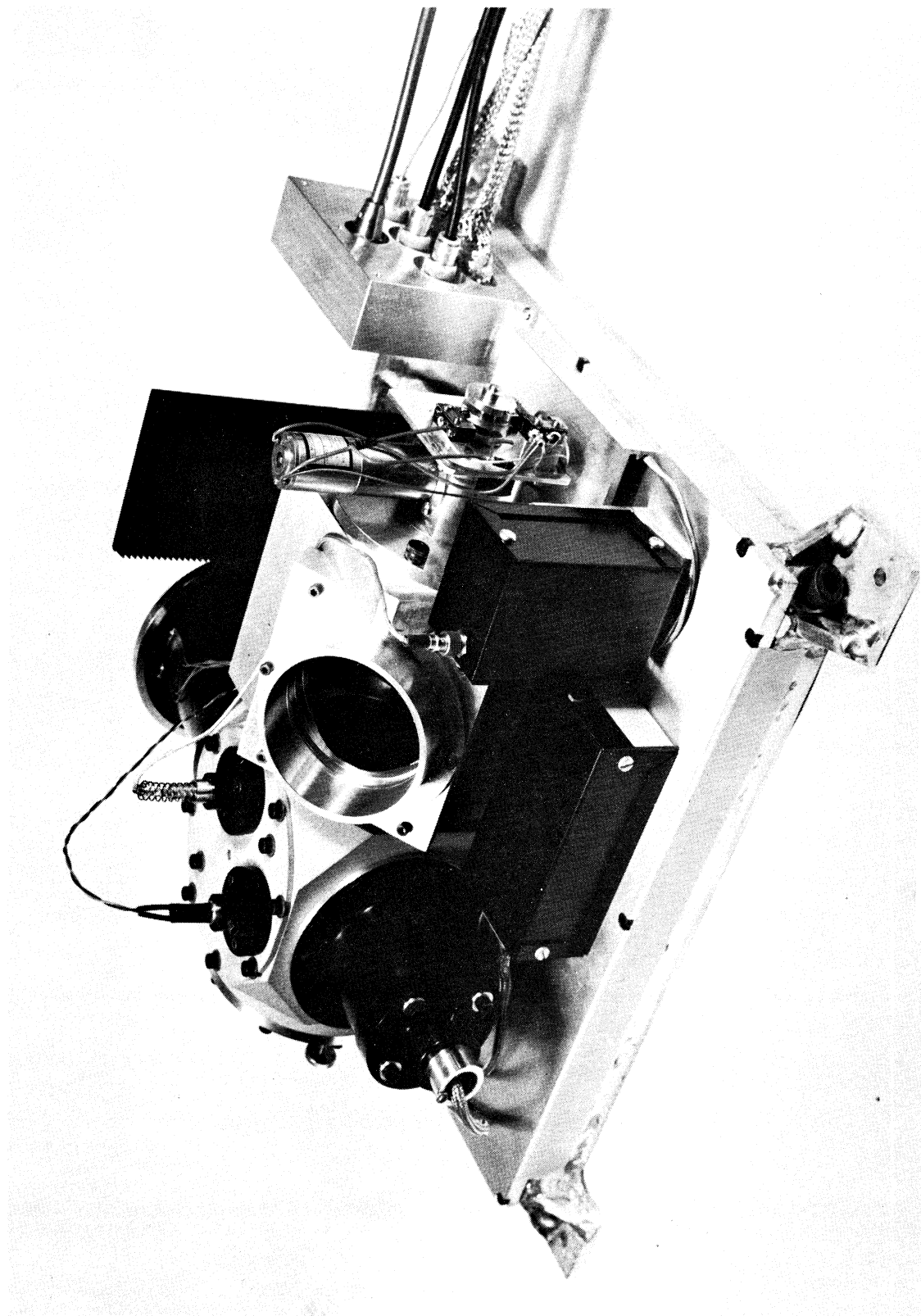
Figure 18. Interferometer, complete optical package.
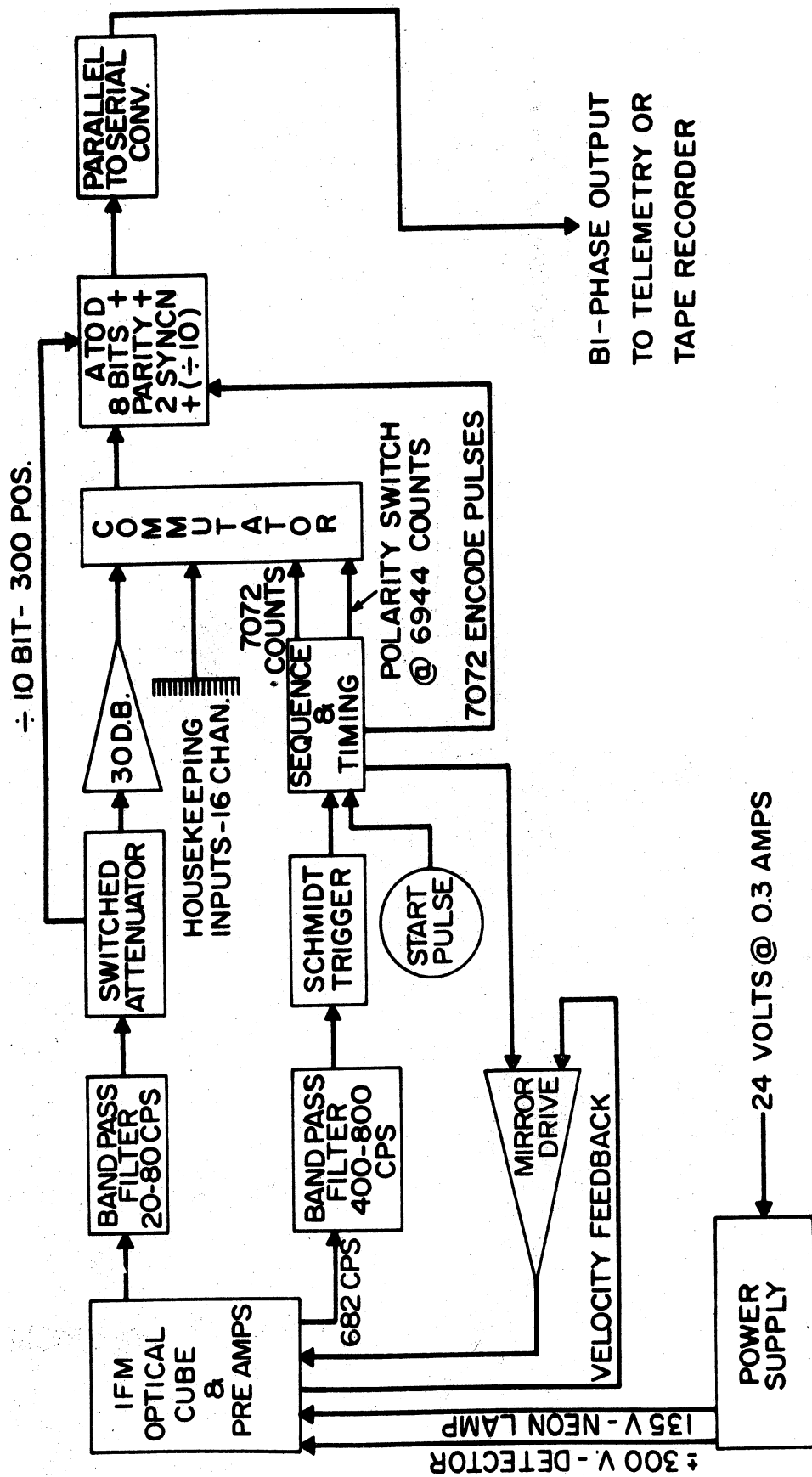
Figure 19. *BALLOON INTERFEROMETER ELECTRONICS BLOCK DIAGRAM*

40
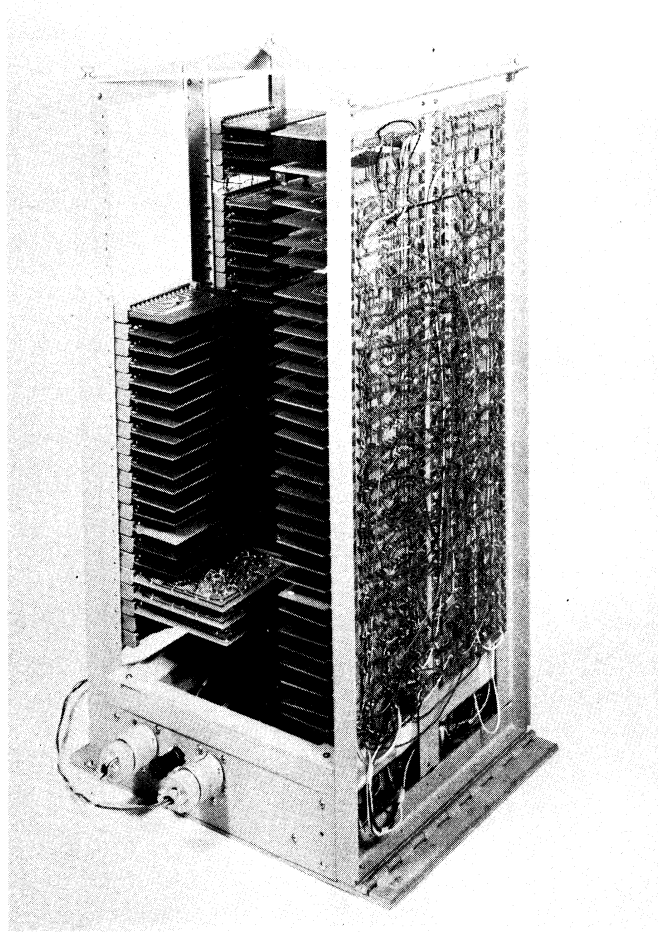
Figure 20. Electronics flight package
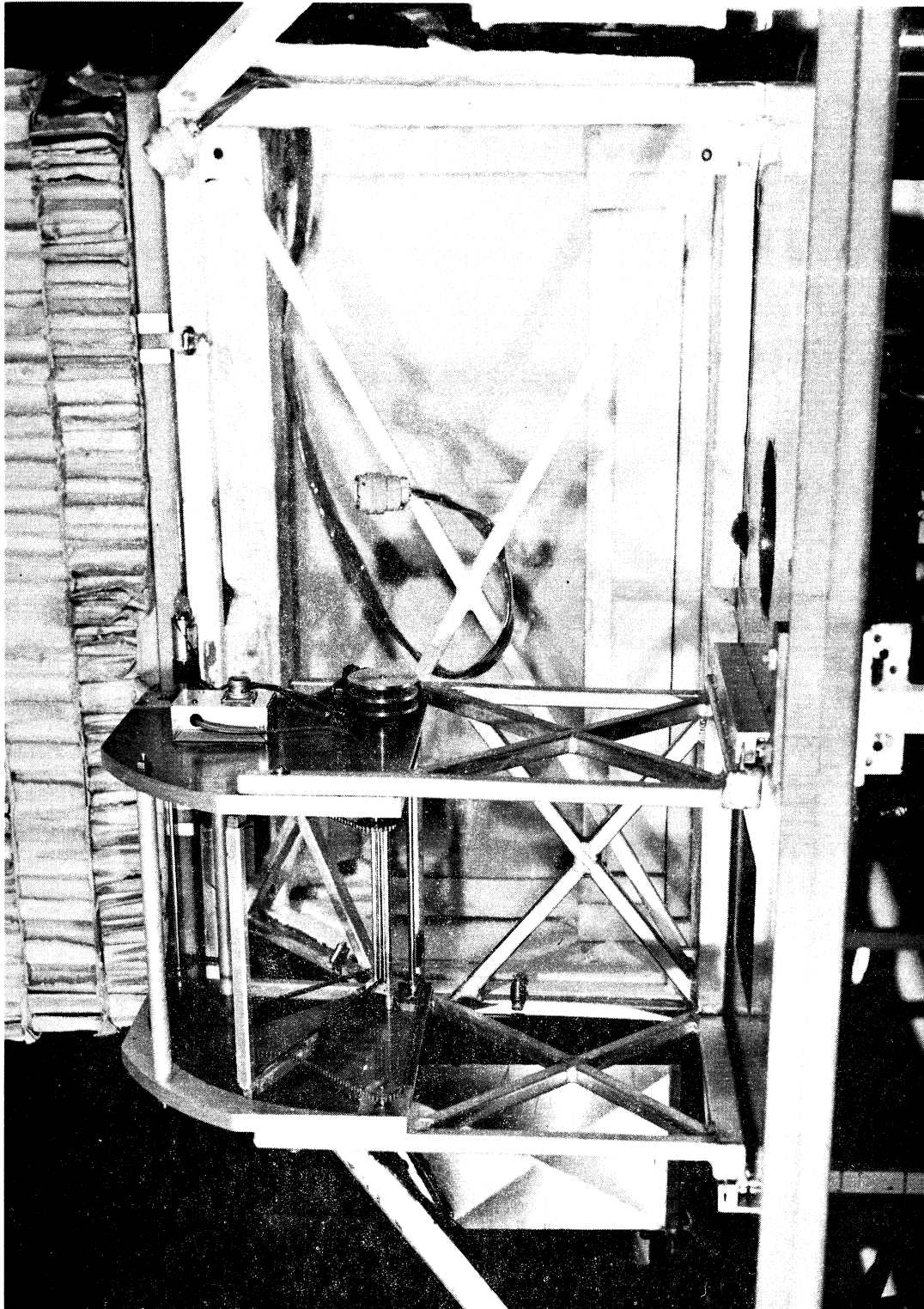
Figure 21. Auxiliary view mirror mounted on gondola
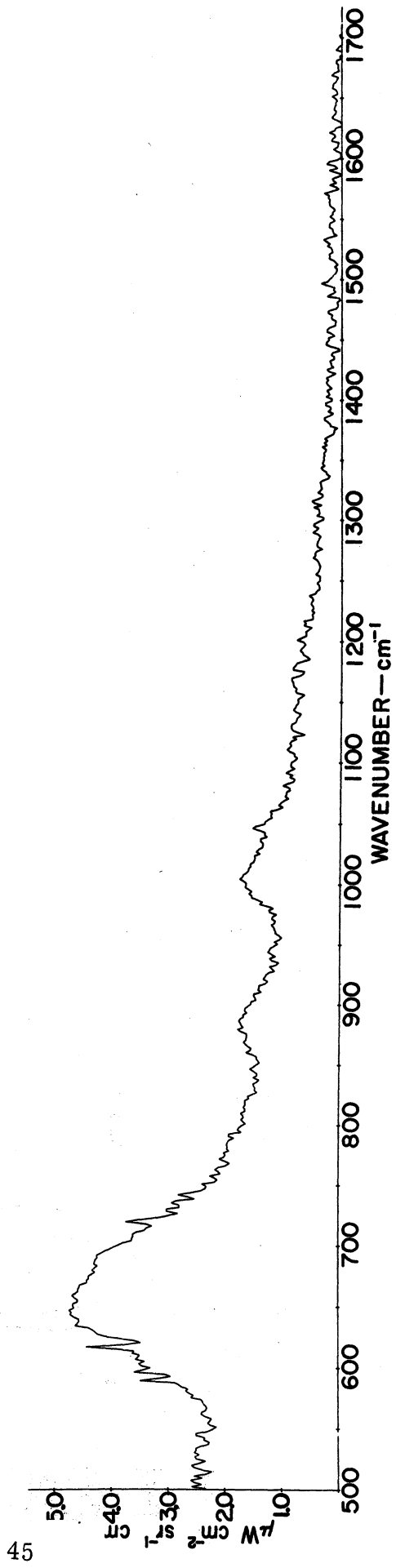
Figure 24.   Atmospheric radiance of horizon at 14:30Z November 20, 1968 balloon altitude 111, 700 feet.

45
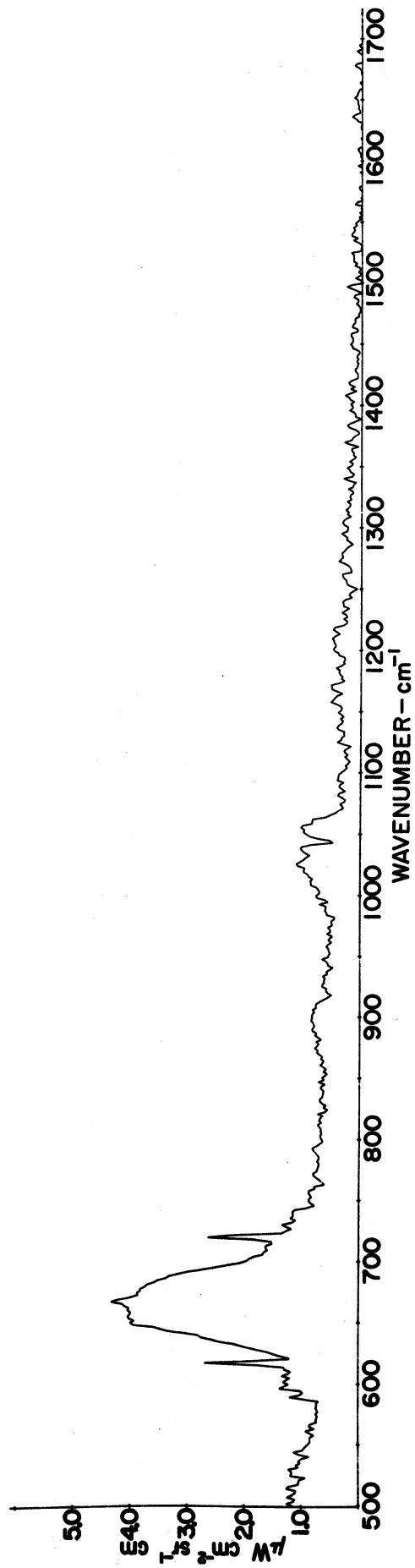
Figure 25.   Atmospheric radiance 22° above horizon at 14:30:32 November 20, 1968 - balloon altitude 111, 700 feet.

46
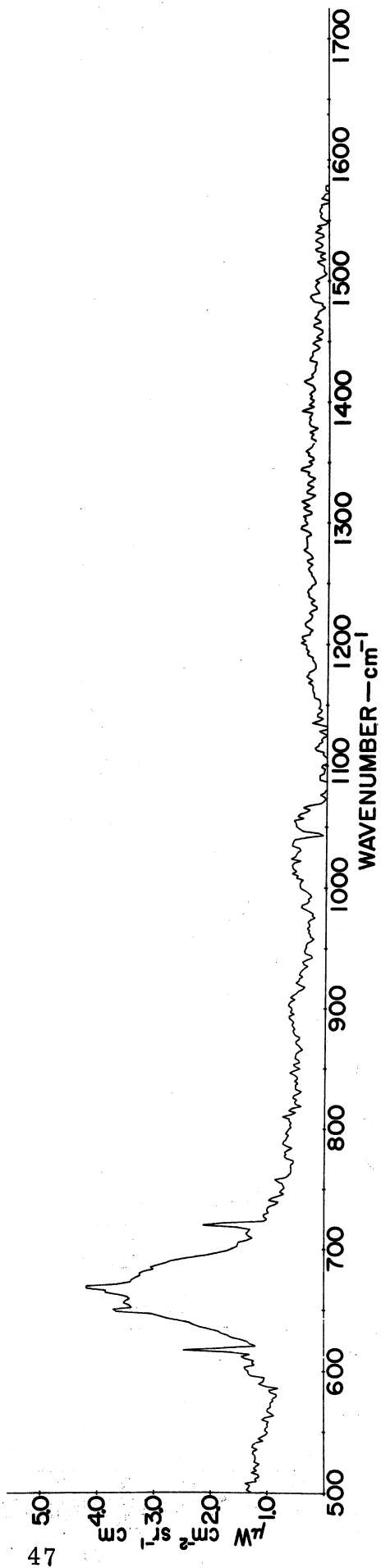
Figure 26. Atmospheric radiance 44° above horizon at 14:31:02Z November 20, 1968
Balloon altitude 111, 700 feet.

47
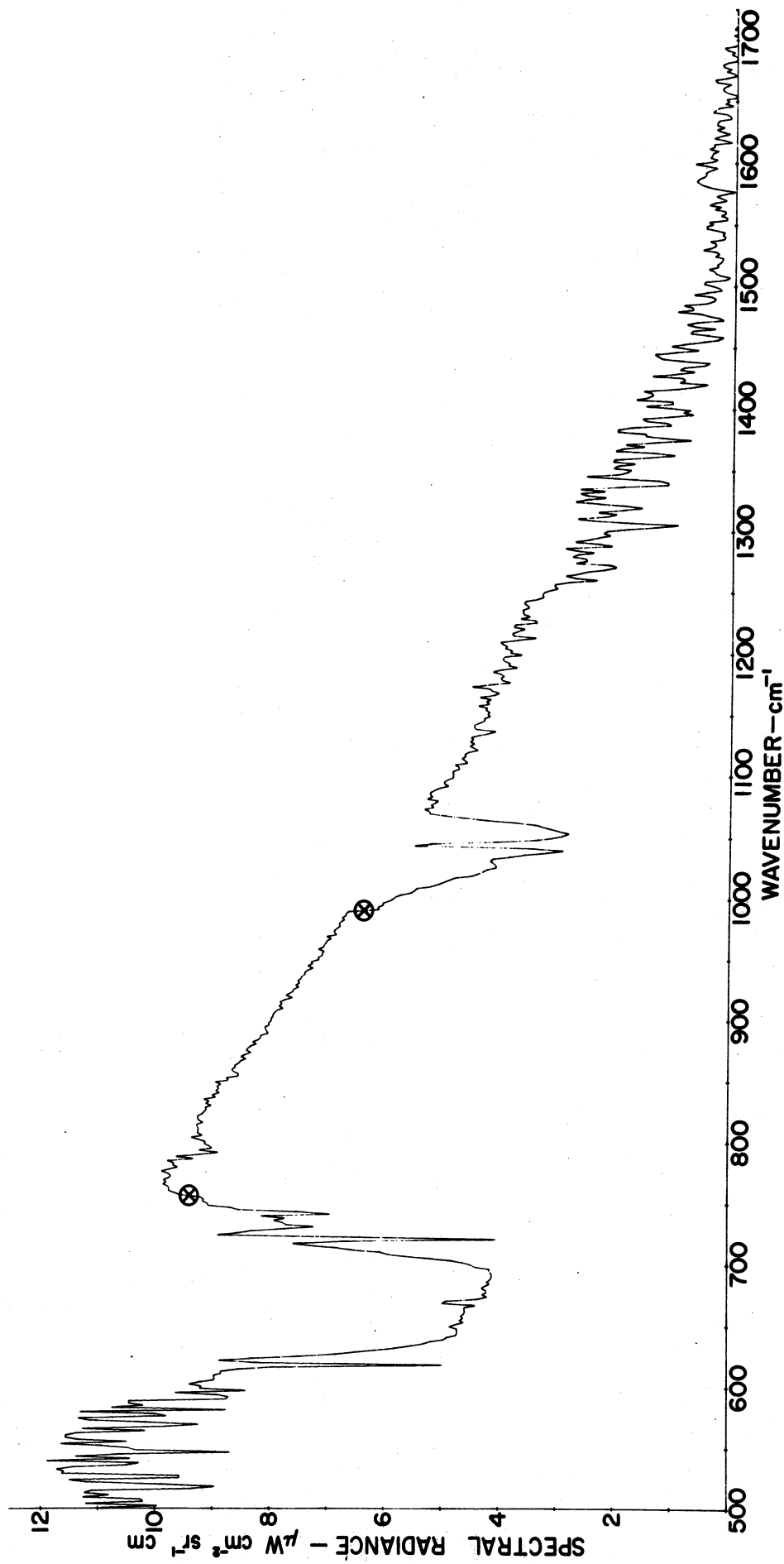
Figure 27. Scene radiance at 15:04:42Z November 20, 1968 rectification errors noted ⊗

48
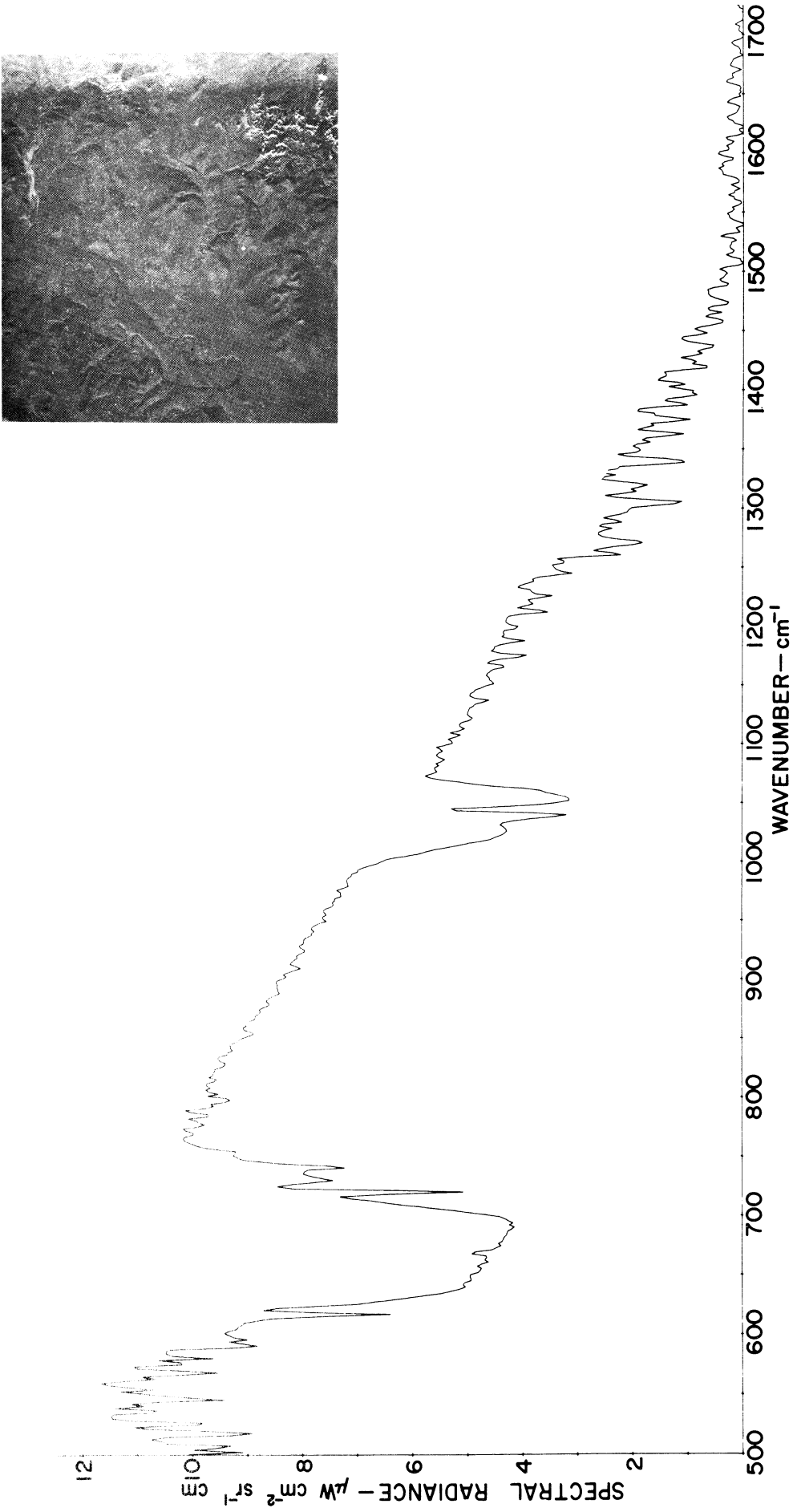
Figure 28. Scene radiance measured 15:47:22Z November 20, 1968.

49
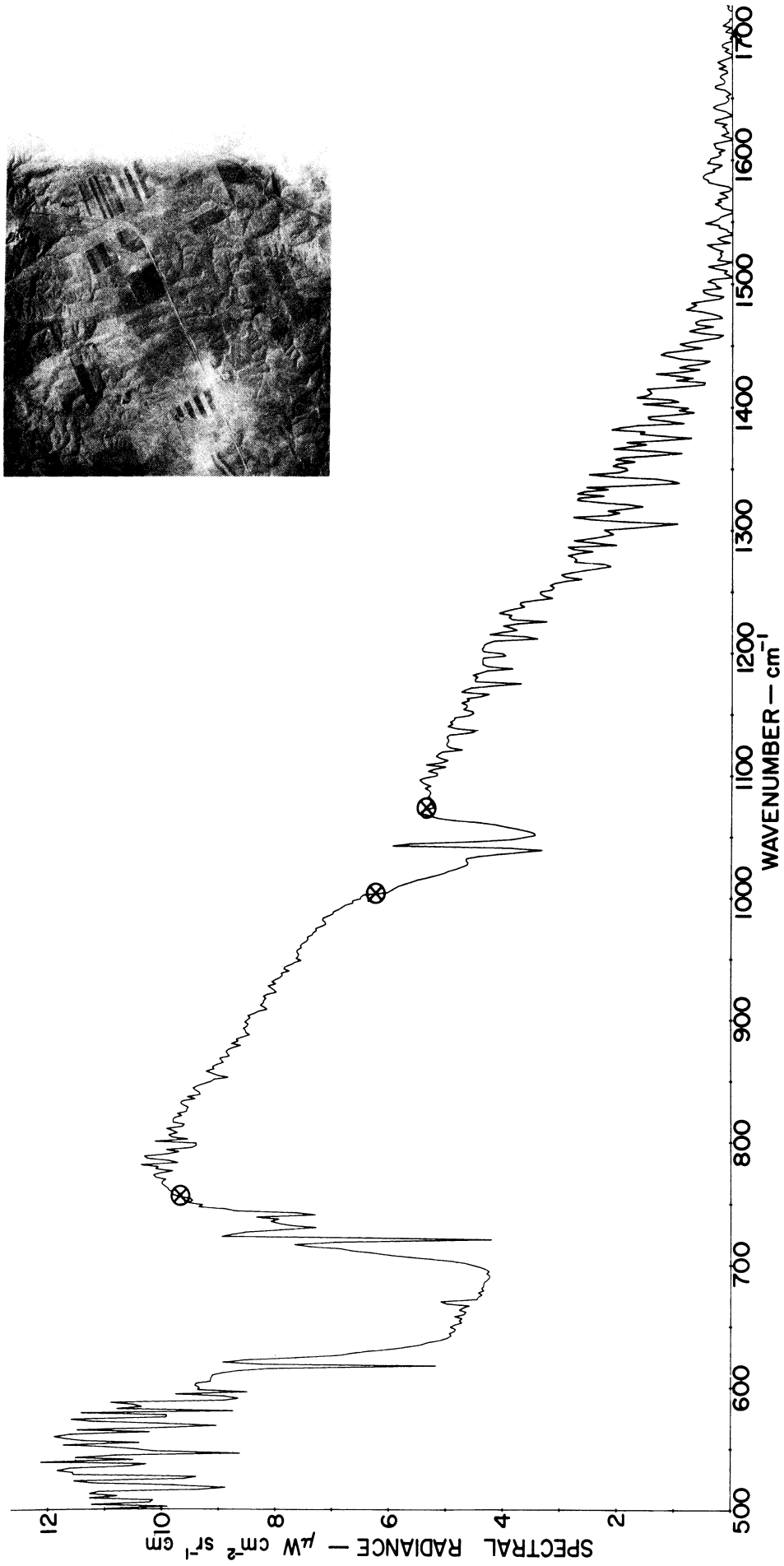
Figure 29. Scene radiance at 16:38:34Z November 20, 1968 rectification errors noted ⊗

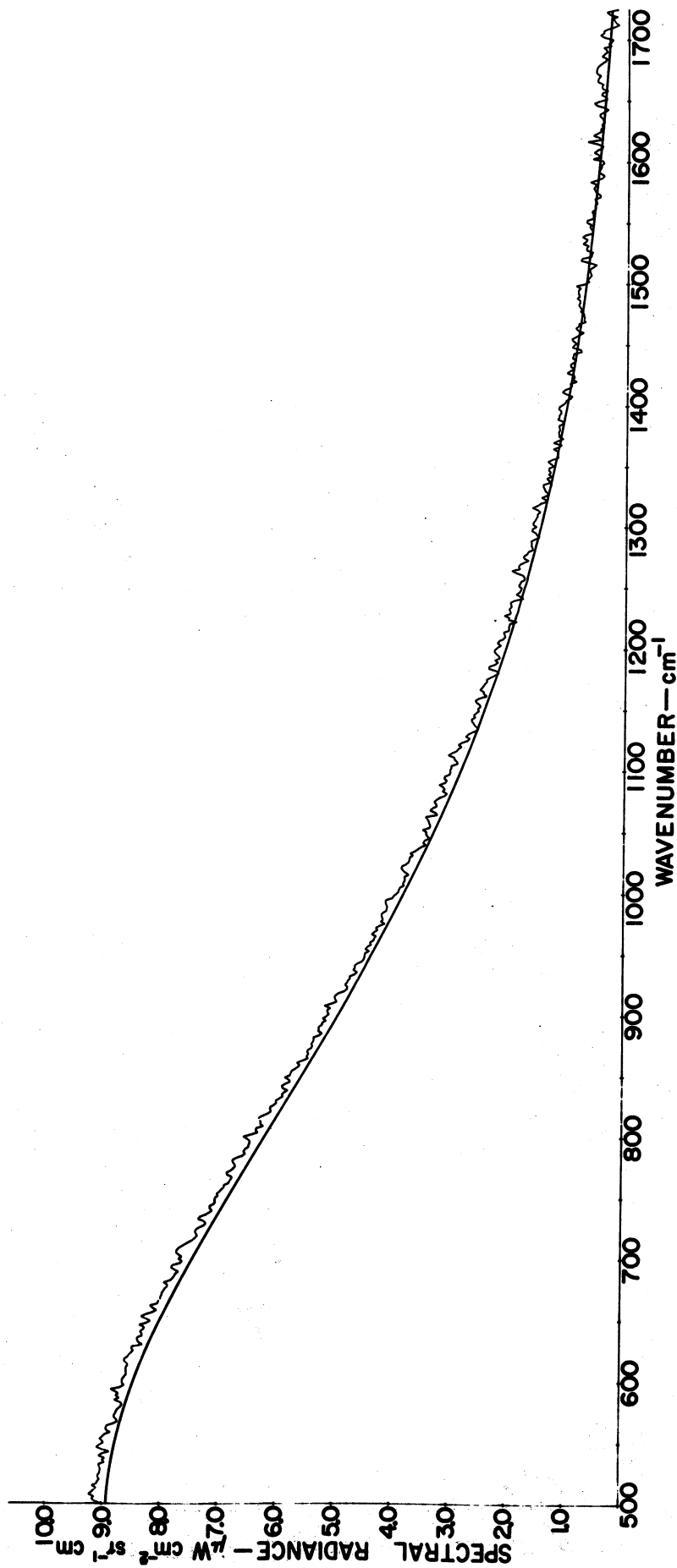50
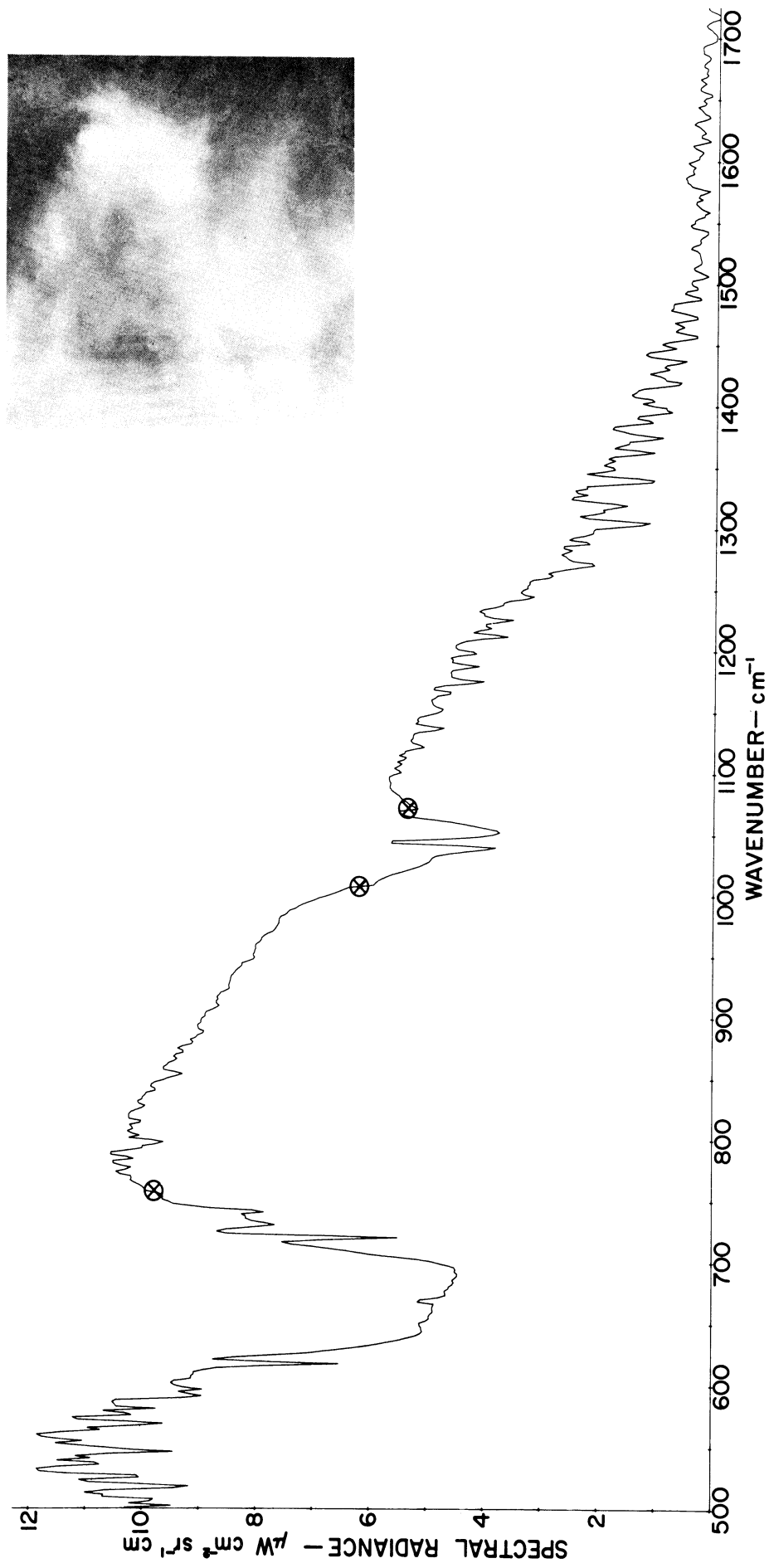
Figure 30. Scene radiance at 17:12:42Z November 20, 1968 rectification errors noted ⊗
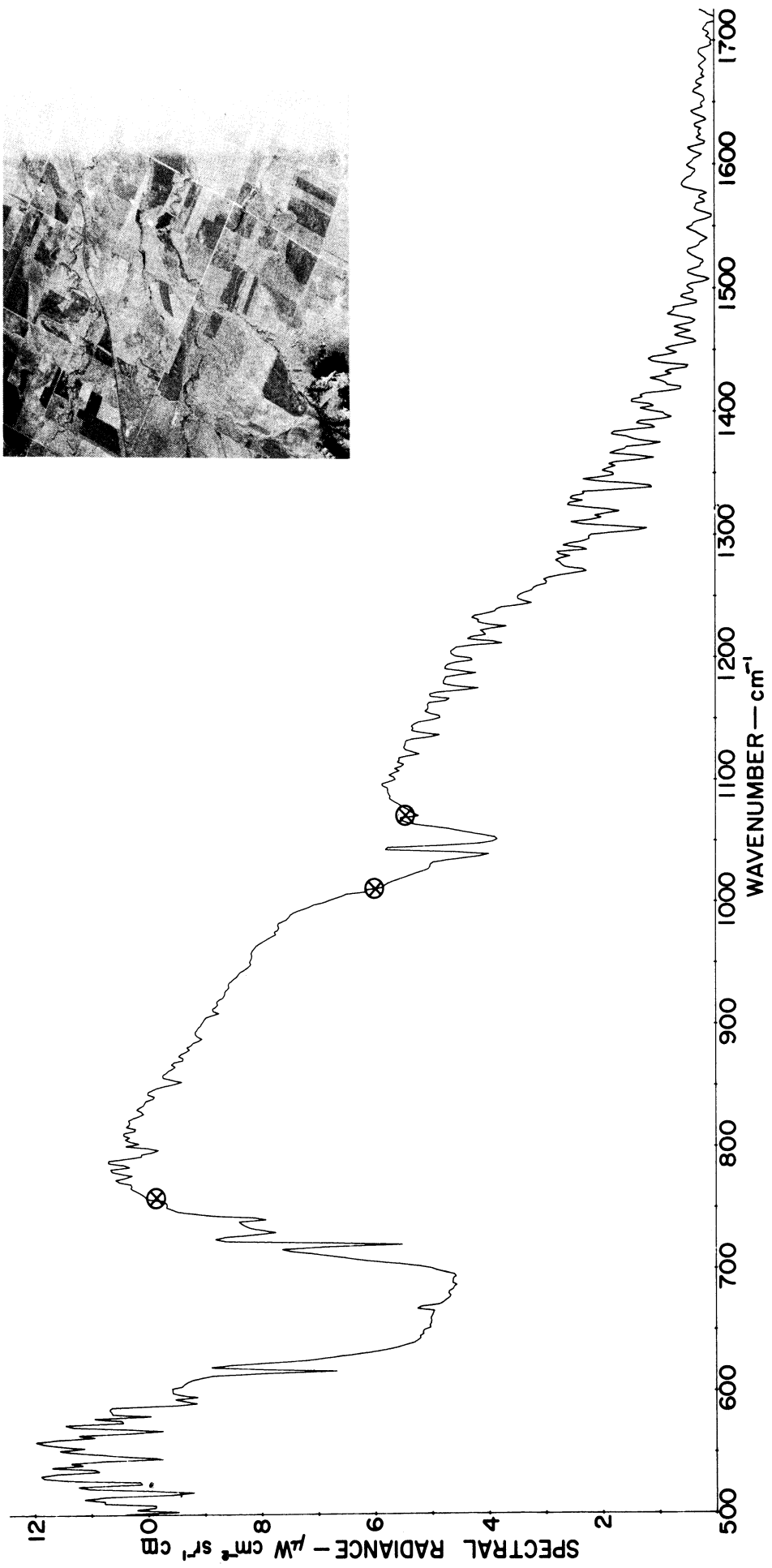
Figure 31. Scene radiance at 18:03:54Z November 20, 1968 rectification errors noted ⊗
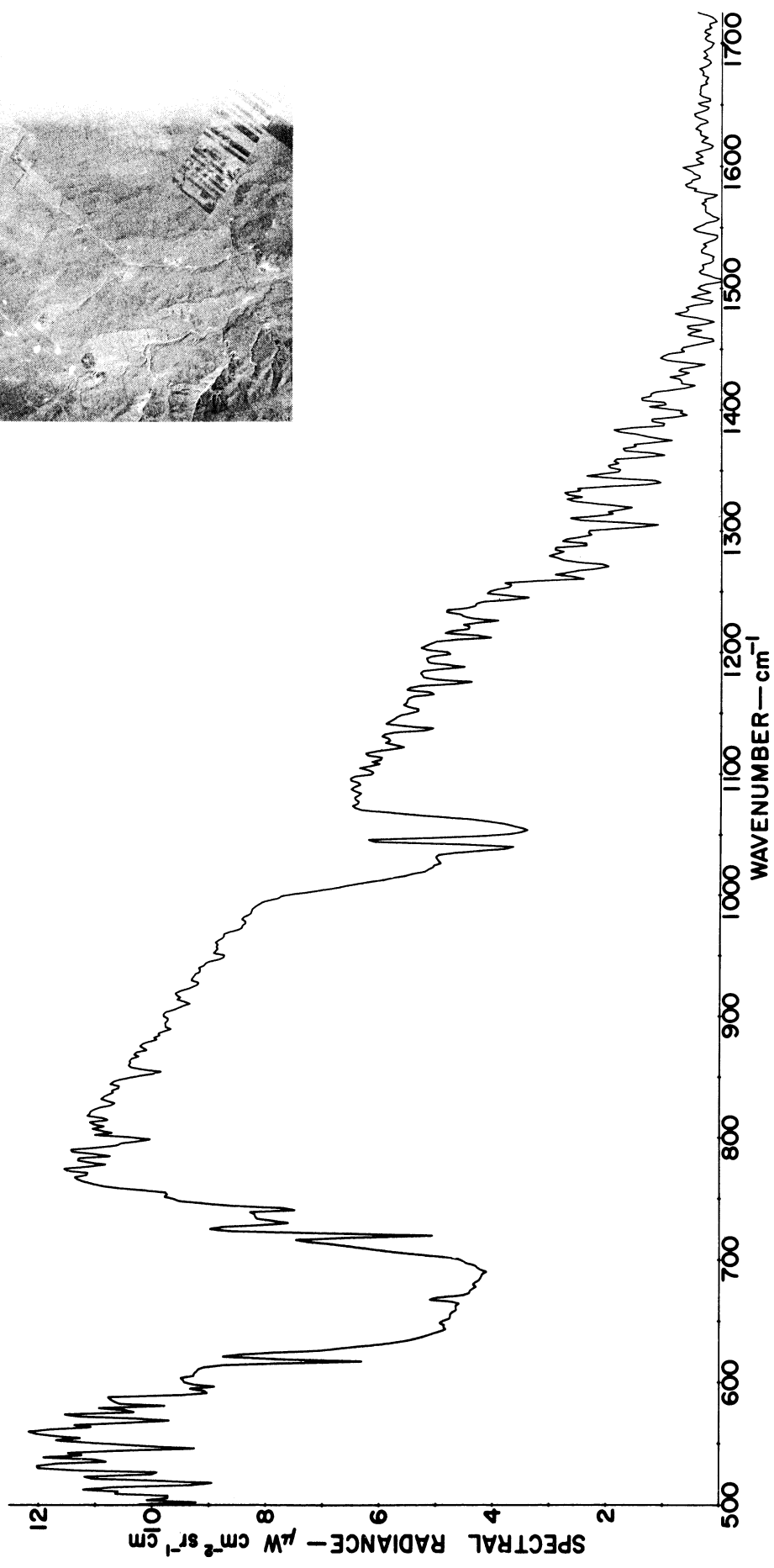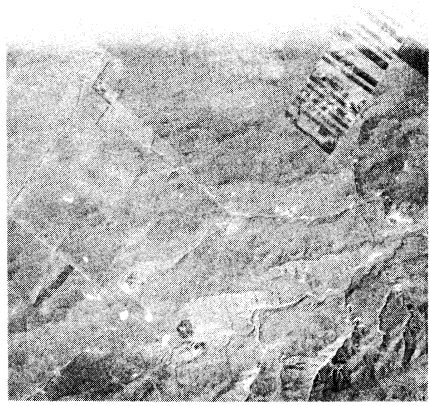
Figure 32. Spectral radiance 19:12:10Z November 20, 1968

Figure 33. Comparison of interferometer measured spectral radiance of cold blackbody and theoretical radiance derived from temperature measurements - first calibration.
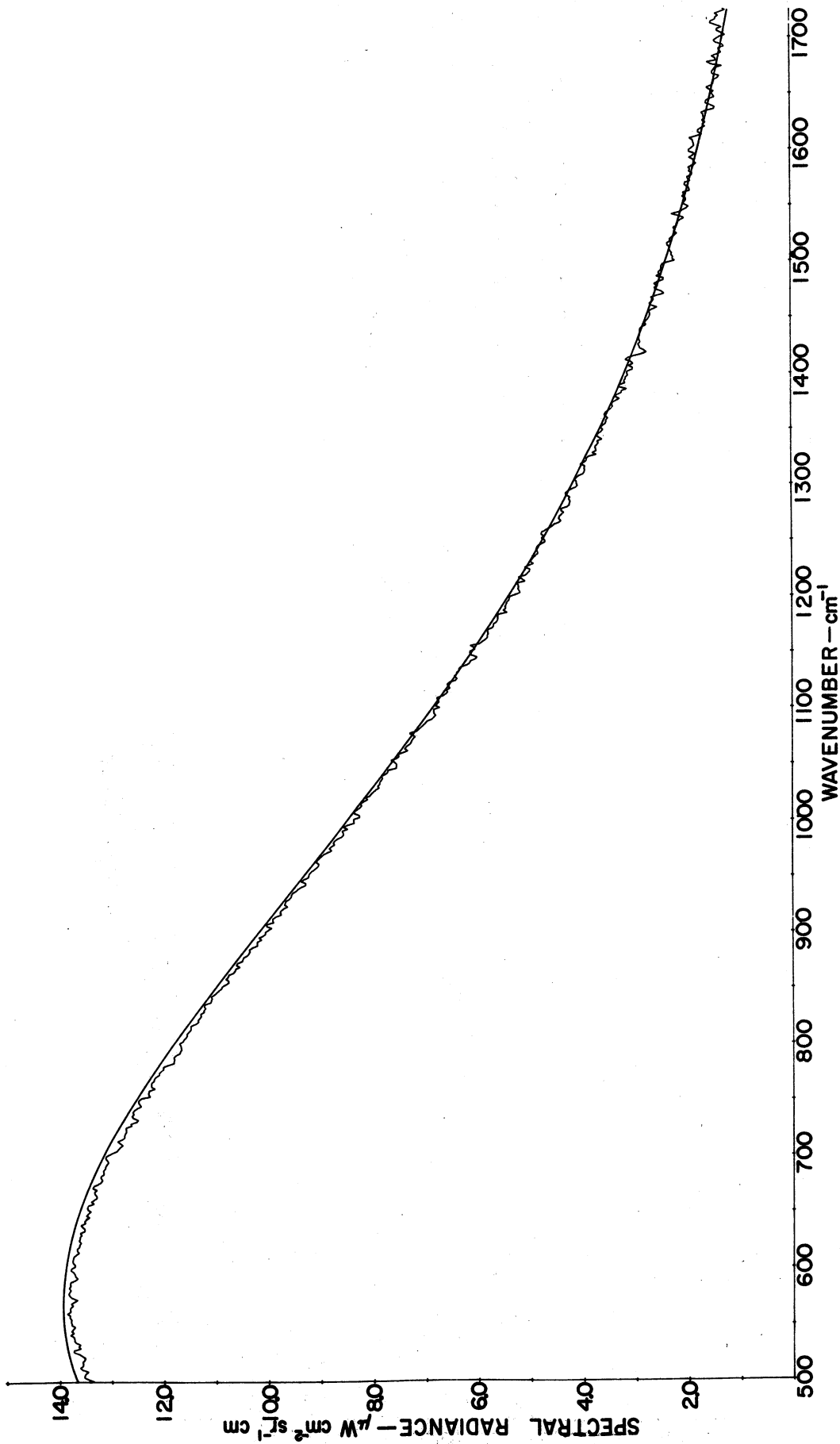
54

Figure 34. Comparison of interferometer measured spectral radiance of warm blackbody and theoretical radiance derived from temperature measurements - first calibration.
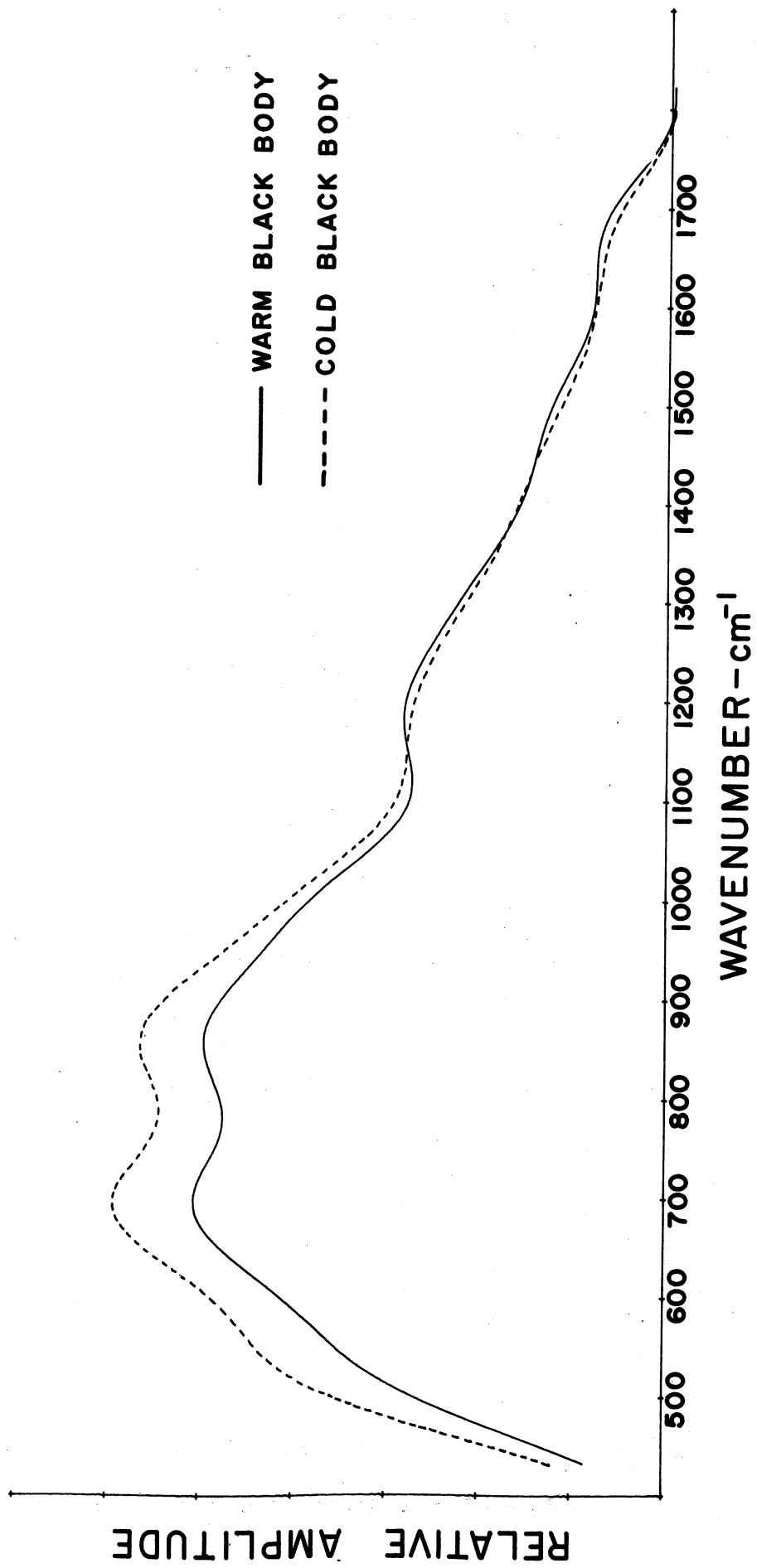
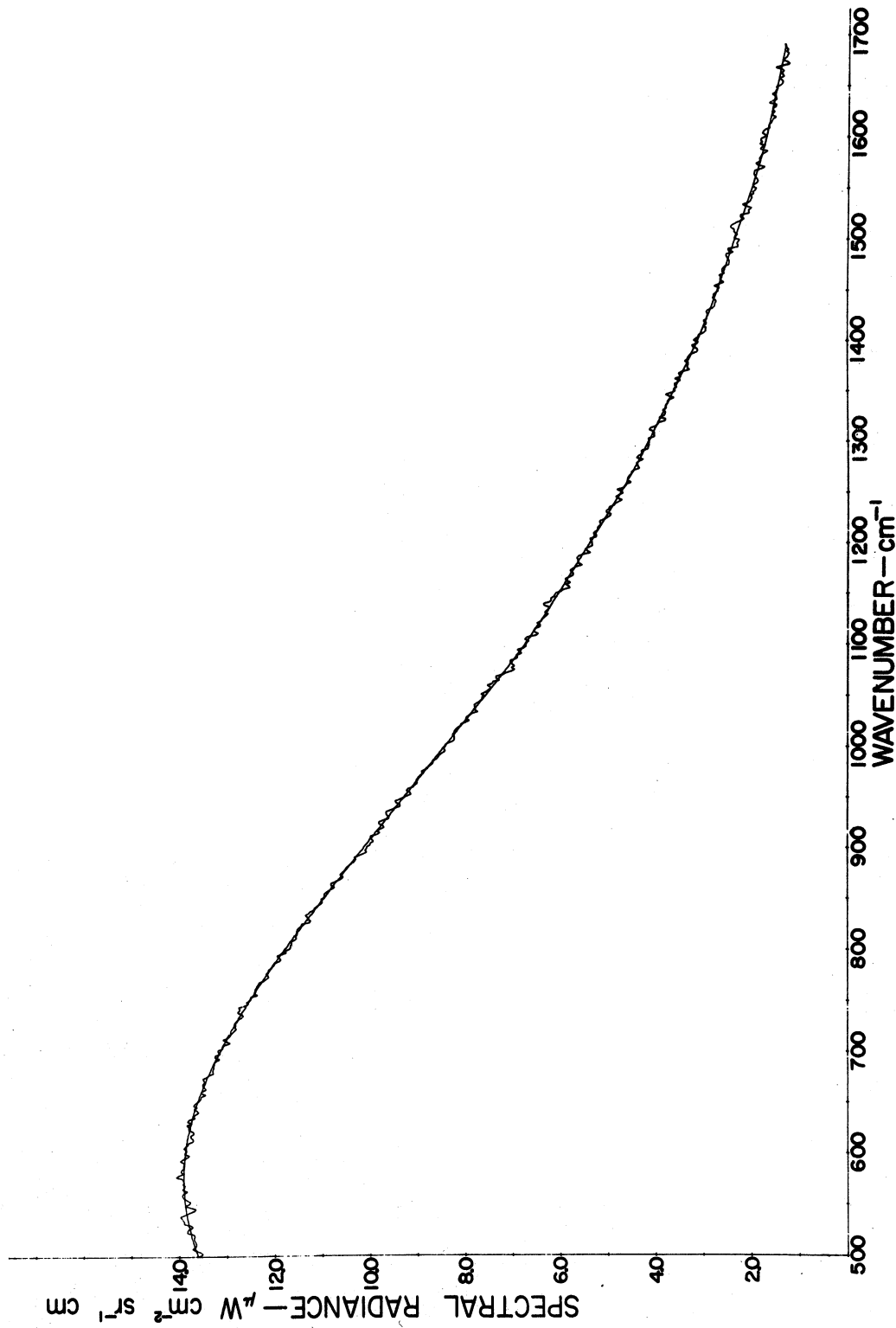Figure 35. Comparison of relative amplitudes of warm and cold blackbodies.

Figure 36. Comparison of interferometer measured spectral radiance of warm
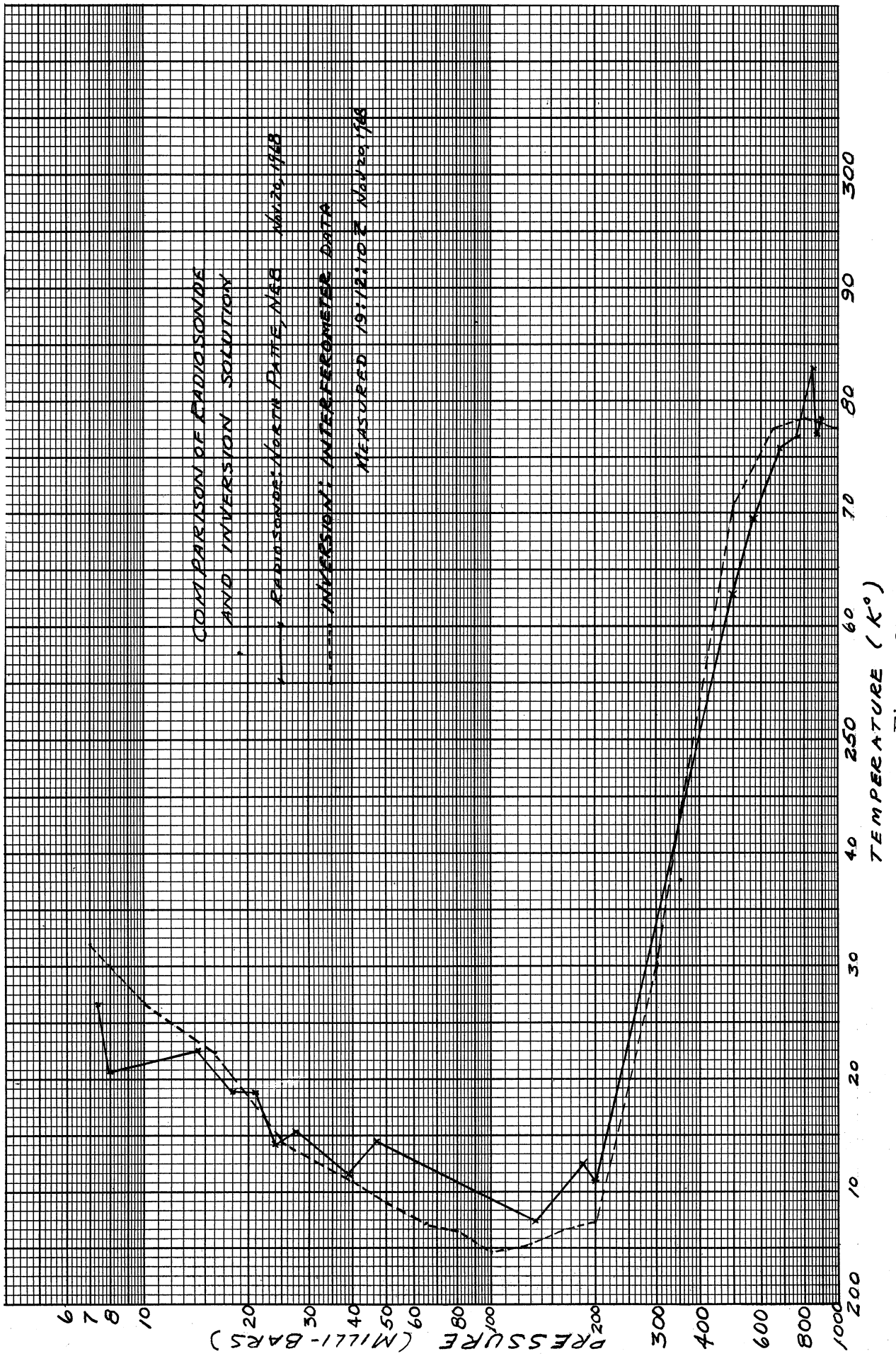blackbody and theoretical radiance derived from temperature measurements -
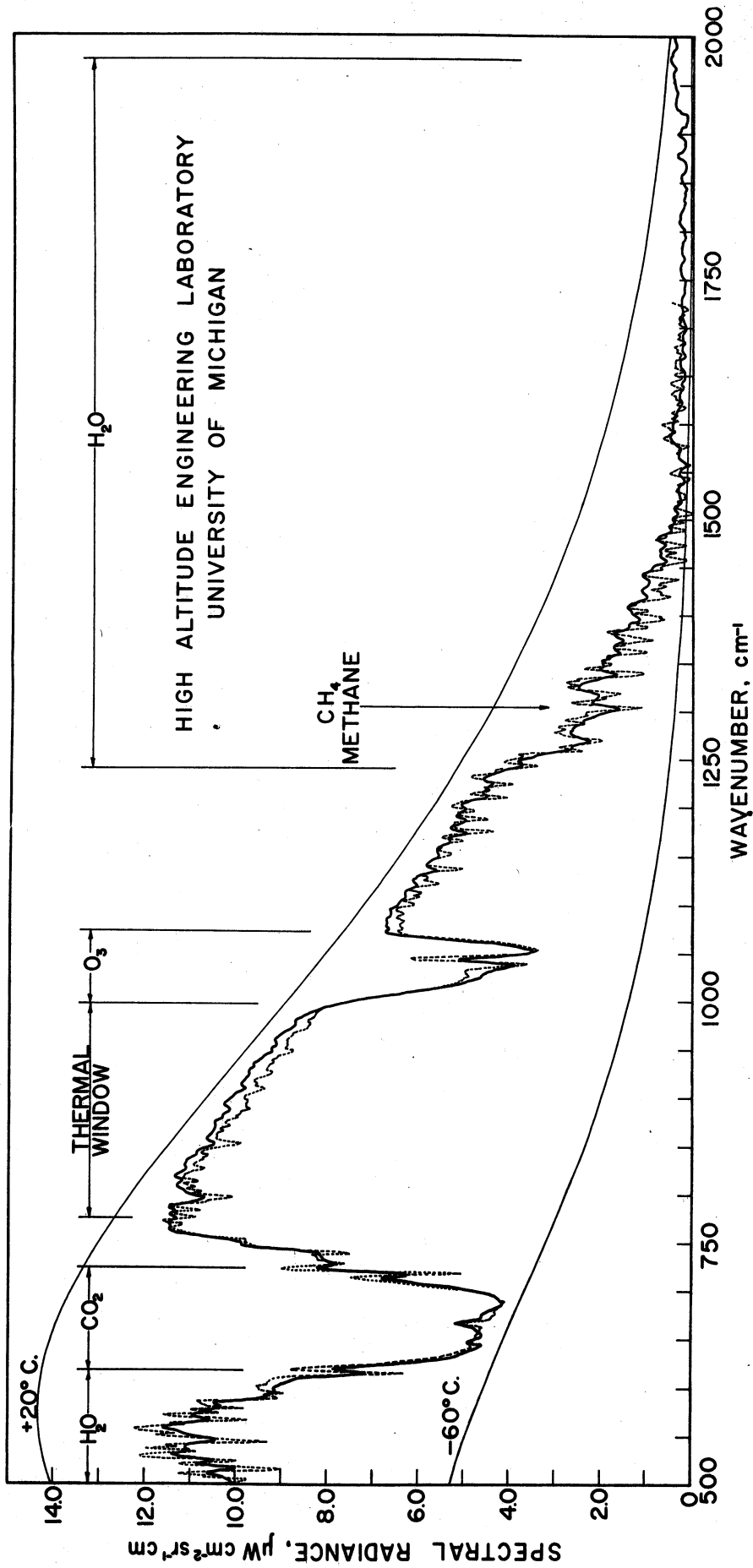second calibration.

57

COMPARISON OF RADIOSONDE
AND INVERSION SOLUTION

⊢——⊣ RADIOSONDE: NORTH DATE: N43   Mar 29,1968

------ INVERSION: INTERFEROMETER DATA

MEASURED 19:12:10 Z   Mar 29,1968

TEMPERATURE (K°)

Figure 37.

PRESSURE (MILLI-BARS)

58

Figure 38. Spectra comparison

(——) May 8, 1966 07:30 CST - Palestine, Tex. - Resolution 5 cm^{-1}

(·····) Nov. 22, 1968 12:12 MST - Rapid City, S. D. Resolution 3 cm^{-1}